Polarimetric Signatures in Supercell Thunderstorms

MATTHEW R. KUMJIAN AND ALEXANDER V. RYZHKOV

Cooperative Institute for Mesoscale Meteorological Studies, University of Oklahoma, and NOAA/OAR/National Severe Storms Laboratory, Norman, Oklahoma

(Manuscript received 14 September 2007, in final form 10 December 2007)

ABSTRACT

Data from polarimetric radars offer remarkable insight into the microphysics of convective storms. Numerous tornadic and nontornadic supercell thunderstorms have been observed by the research polarimetric Weather Surveillance Radar-1988 Doppler (WSR-88D) in Norman, Oklahoma (KOUN); additional storm data come from the Enterprise Electronics Corporation "Sidpol" C-band polarimetric radar in Enterprise, Alabama, as well as the King City C-band polarimetric radar in Ontario, Canada. A number of distinctive polarimetric signatures are repeatedly found in each of these storms. The forward-flank downdraft (FFD) is characterized by a signature of hail observed as near-zero Z_{DR} and high Z_{HH}. In addition, a shallow region of very high Z_{DR} is found consistently on the southern edge of the FFD, called the Z_{DR} "arc." The Z_{DR} and K_{DP} columns and midlevel "rings" of enhanced Z_{DR} and depressed ρ_{HV} are usually observed in the vicinity of the main rotating updraft and in the rear-flank downdraft (RFD). Tornado touchdown is associated with a well-pronounced polarimetric debris signature. Similar polarimetric features in supercell thunderstorms have been reported in other studies. The data considered here are taken from both S- and C-band radars from different geographic locations and during different seasons. The consistent presence of these features may be indicative of fundamental processes intrinsic to supercell storms. Hypotheses on the origins, as well as microphysical and dynamical interpretations of these signatures, are presented. Implications about storm morphology for operational applications are suggested.

1. Introduction

Because of the severity and high-impact nature of supercells, these storms have been intensely studied for several decades. Both the majority of significant tornadoes (Doswell 2001) and about 90% of hail greater than 5 cm in diameter (Thompson et al. 2003) are associated with supercell thunderstorms. Additionally, supercells can cause damaging winds and flooding rains (Doswell 1994; Smith et al. 2001).

Past observational studies of supercells have mainly emphasized storm structure and dynamics as well as high-impact phenomena, such as hail and tornadoes. In early studies of airflow patterns and storm structure, the temporal evolution of radar reflectivity echoes (e.g., Browning 1964, 1965; Marwitz 1972) and winds revealed by dual-Doppler analyses (e.g., Lemon and Doswell 1979; Brandes 1977, 1978, 1981, 1984a,b; Brandes et al. 1988) were utilized to develop conceptual models of supercell evolution. These studies provided some of the defining characteristics of supercells, including the reflectivity "hook" echo, the persistent, strong updraft and mesocyclone, and the forward-flank downdrafts (FFDs) and rear-flank downdrafts. For a review of rear-flank downdrafts and hook echoes, see Markowski (2002). More recently, mobile radars (e.g., Bluestein et al. 1995; Wurman et al. 1997; Biggerstaff et al. 2005) and airborne Doppler radars (e.g., Bluestein and Gaddy 2001; Cai and Wakimoto 2001) have been used in conjunction with ground-based Doppler radars to provide finer spatial resolution and coverage of supercell storms. These multiple-Doppler analyses have revealed the three-dimensional wind flow within supercells, from which the distributions of vertical velocity, vorticity, and pressure perturbations have been retrieved. Studies including Miller et al. (1988) have used the retrieved wind fields to calculate trajectories of air parcels and hailstones. Additionally, in situ measurements using mobile mesonet stations have yielded ob-

Corresponding author address: Matthew R. Kumjian, CIMMS/NSSL, National Weather Center, 120 David L. Boren Blvd., Norman, OK 73072.
E-mail: matthew.kumjian@noaa.gov

DOI: 10.1175/2007JAMC1874.1

servations of the low-level thermodynamic structure near supercells (e.g., Straka et al. 1996; Markowski et al. 2002; Shabbott and Markowski 2006; Grzych et al. 2007).

Numerical simulations of supercells have also facilitated our understanding of storm structure and morphology. The pioneering studies of Klemp and Wilhelmson (1978) and Rotunno and Klemp (1982, 1985) provided insight into the origins of updraft rotation, storm splitting, shear-induced pressure perturbations, and other observed supercell characteristics. Using a more sophisticated and higher-resolution numerical model, Adlerman et al. (1999) simulated cyclic mesocyclogenesis. As model resolution increases and computational expense decreases, simulations of supercell tornadoes and tornadogenesis (e.g., Wicker and Wilhelmson 1995) are becoming more common in the literature.

However, in contrast to the large body of work on the dynamics of such storms, relatively little attention has been focused on supercell microphysics. This is partly due to the lack of observational capabilities, because flying aircraft into supercells can be extremely dangerous and conventional single-polarization radars are not adequate for microphysics studies. Moreover, storm-scale numerical simulations typically employ bulk microphysics parameterization schemes and thus cannot adequately model storm microphysical processes. However, the relatively recent tool of dual-polarization radar can potentially offer remarkable insight into the microphysics of severe convective storms. There have been numerous observational case studies of supercells (e.g., Conway and Zrnić 1993; Hubbert et al. 1998) and severe nonsupercellular storms (e.g., Bringi et al. 1986; Zrnić et al. 1993; Höller et al. 1994; Kennedy and Rutledge 1995; Kennedy et al. 2001) using polarimetric radars. Additionally, polarimetric radars have been used in conjunction with in situ aircraft measurements of supercells (e.g., Loney et al. 2002; Schlatter 2003) and severe nonsupercell storms (e.g., Bringi et al. 1984, 1991, 1996; Brandes et al. 1995). Despite being limited by very small sample sizes (most of the above-mentioned papers only analyze one or two storms), the use of polarization diversity in these studies provides an intriguing and powerful method of observing supercells, from which inferences can be made about microphysical processes within the storm.

Recent work by Van Den Broeke et al. (2008) analyzes multiple supercell cases. They present a preliminary climatology of polarimetric characteristics of southern Great Plains classic supercells, describing the temporal evolution of the polarimetric variables for several tornadic storms. In contrast, the present study considers a much larger dataset, including both tornadic and nontornadic supercells observed in different climate regions, different seasons, and at S and C bands. Additionally, it covers a spectrum of supercell types, including classic, high precipitation (HP), and low precipitation (LP), as defined by Rasmussen and Straka (1998). The purpose of this paper is to draw attention to several distinct and repetitive signatures seen in most supercells, and to provide possible explanations for the origin of these signatures. The potential significance of these signatures for diagnosing storm behavior and operational applications are also presented.

TABLE 1. Storm cases analyzed in this study. The date and time (UTC) are given, along with whether the storm was tornadic (T) or nontornadic (N). The asterisk (*) indicates that the data come from the Sidpol C-band polarimetric radar in Enterprise and the cross (+) indicates data from the King City C-band polarimetric radar. All other cases are from the S-band KOUN in Norman.

Date	T/N	Time of observation (UTC)
8 May 2003	T	2145–2329
7–8 May 2003	N	0358–0555
10 May 2003	T	0120–0457
19–20 May 2003	N	2303–0107
26–27 May 2004	N	2236–0038
29–30 May 2004	T	2159–0630
10 Nov 2004	T	2208–0018
10–11 Apr 2005a	T	2247–0207
10–11 Apr 2005b	N	0039–0207
19 Aug 2005+	T	1740
13 Sep 2005	N	0044–0209
15 Nov 2006*	N	1803
1 Mar 2007*	T	1824–1932
29 Mar 2007	T	2047–2125
10 Apr 2007	N	2257–0053
7 May 2007	T	0201–0247
9 May 2007	T	0002–0126
9 May 2007	T	0358–0502

In this study, 14 supercell thunderstorms observed by the polarimetric prototype of the Weather Surveillance Radar-1988 Doppler (WSR-88D) S-band radar in Norman, Oklahoma (KOUN), are analyzed. Additional data from the Enterprise Electronics Corporation (EEC) Sidpol C-band dual-polarization radar in Enterprise, Alabama, and from the King City C-band dual-polarization radar in Ontario, Canada, are utilized. Data are analyzed throughout the lifetime of 15 supercell thunderstorms, of which 9 were tornadic (including one from Alabama) and 6 were nontornadic. Several nonsupercell tornadic storms are also analyzed. The dates and times of the analyzed storms are given in Table 1. The polarimetric radar variables that were utilized in this study are radar reflectivity factor at horizontal polarization (Z_{HH}), differential reflectivity

(Z_{DR}), the magnitude of the copolar cross-correlation coefficient [$|\rho_{HV}(0)|$; herein ρ_{HV}], Doppler velocity (v_r), and specific differential phase (K_{DP}). For a review of the polarimetric variables and the utility of polarimetric radar data in meteorological applications, see Balakrishnan and Zrnić (1990), Herzegh and Jameson (1992), Doviak and Zrnić (1993), Zrnić and Ryzhkov (1999), and Bringi and Chandrasekar (2001).

Here we only briefly summarize physical meaning of the polarimetric variables. Differential reflectivity is a good measure of the median size of raindrops. The Z_{DR} of ice particles with the same shape and orientation as raindrops is much lower than the corresponding Z_{DR} in rain. Similarly to Z_{DR}, specific differential phase is affected by the shape and orientation of hydrometeors and is much lower for ice particles than for raindrops (except for low-reflectivity ice crystals). As opposed to Z_{DR}, K_{DP} is directly proportional to particle concentration and, therefore, is correlated with Z_{HH} (but only in rain and melting hail). The cross-correlation coefficient is close to one for most atmospheric hydrometeors and is substantially lower for the nonmeteorological echo caused by ground clutter, biological scatterers, and tornadic debris. However, ρ_{HV} noticeably drops for hydrometeors with "resonance" sizes for which the ratio $D|\varepsilon|^{1/2}/\lambda$ approaches 1, where D is the equivolume diameter, ε is the dielectric constant, and λ is the radar wavelength. This usually happens for large raindrops at C band ($D > 5$ mm) as well as large, wet snowflakes in the bright band and wet hailstones at all microwave frequencies. The magnitude of ρ_{HV} also tends to decrease for the more chaotic orientation of nonspherical scatterers.

The volume scans are composed of 14 or 15 elevation angle scans ranging from 0.0° (or 0.5°) to about 19.5°, according to a standard WSR-88D scanning strategy. To assess the three-dimensional structure of the storm, data from each volume scan undergo a Delaunay triangulation scheme and are linearly interpolated onto a three-dimensional Cartesian grid with 500-m horizontal resolution, from which constant-altitude plan position indicators (CAPPIs) are produced for every 250 m in the vertical, from near the ground to the echo top (if available in the data). For graphical purposes, polar surfaces of individual plan position indicator (PPI) scans are similarly interpolated onto a Cartesian grid. No advection correction schemes are applied; despite this limitation, in addition to the errors possibly introduced by the linear interpolation from polar surfaces to a Cartesian grid, useful qualitative analyses are possible. For quantitative analysis, conical scan data on the original spherical polar surfaces are used. Three-dimensional quantitative analysis generally requires the utilization of advection correction schemes (e.g., Gal-Chen 1982). A similar objective analysis is used for the data at C band, as will be explained in a later section.

The next section will describe the repetitive polarimetric signatures found in supercell storms, with a subsection devoted to describing each signature in detail. Section 3 will provide an example case observed at S band, briefly highlighting the evolution of the polarimetric signatures as related to the storm evolution. A discussion on C-band measurements and signatures with several examples are presented in section 4. Section 5 includes a discussion of the applicability of identifying and tracking these polarimetric features and conclusions that can be made from this study.

2. Polarimetric signatures

A number of repetitive polarimetric signatures are found in the supercell storms examined herein. These features include the tornadic debris signature (TDS) associated with tornado touchdown, hail signatures near the ground, the Z_{DR} "arc" at low levels, reduced ρ_{HV} in the storm-inflow region at low levels and in the updraft, Z_{DR} and K_{DP} columns extending above the melting layer, and midlevel "rings" of enhanced Z_{DR} and decreased ρ_{HV}. These features are depicted in a conceptual diagram (Fig. 1). It should be noted that the TDS is only present in the tornadic supercells (i.e., there are no "false alarms"). Each of the above-mentioned signatures will be described in more detail in the following subsections.

a. Tornadic debris signature

Ryzhkov et al. (2002) first noted a pronounced polarimetric signature at the tip of the hook echo in a supercell associated with lofted tornadic debris from a damaging tornado on the 3 May 1999 central Oklahoma outbreak. Subsequent studies have shown that the TDS is found consistently at S band and that it could be used for tornado detection (Ryzhkov et al. 2005a). Additionally, the TDS has been documented at C (Ryzhkov et al. 2007a) and X (Bluestein et al. 2007) band. The signature is present when tornadoes loft debris because the random orientation, irregular shape, large size, and high dielectric constant of debris results in high Z_{HH}, low Z_{DR}, and anomalously low ρ_{HV}. Generally a Doppler velocity vortex signature is collocated with the TDS. An example of the TDS from the 10 May 2003 supercell is given in Fig. 2.

Typically, the debris signature is observable at relatively close ranges. At greater distances, the broadening of the beam causes the radar resolution volume to become large enough that it may not resolve the signa-

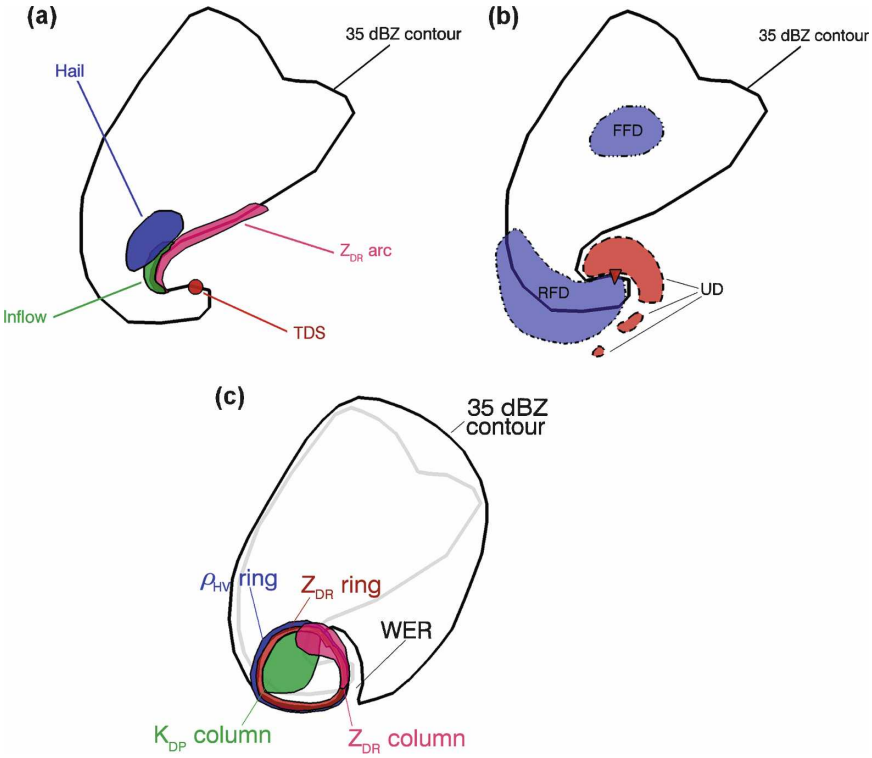

FIG. 1. Schematics of supercell thunderstorms with the locations of features in (a) the polarimetric variables at low levels (<1 km), (b) vertical velocities (adapted from Lemon and Doswell 1979), and (c) polarimetric variables at midlevels (~5 km). In (a), "TDS" is the tornadic debris signature, "hail" is the low-level signature of hail reaching the ground, "inflow" is the low-level inflow signature, and the thick black line is the 35-dBZ contour. In (b), downdrafts are indicated by blue shading and updrafts with red shading. The tornado is indicated by the red triangle. In (c), "WER" is the weak-echo region and the gray outline shows the location of the low-level 35-dBZ contour.

ture. Weaker tornadoes or tornadoes over open fields may not loft debris to heights observable by the radar. Operationally, the TDS may be used to verify warnings and to pinpoint the tornado location. By confirming the presence of a tornado it can alert forecasters that a particular storm has a history of producing tornadoes and thus may be used as a nowcasting tool, giving forecasters high confidence that the nearby environment is favorable for tornadoes.

Ryzhkov et al. (2005a) reports that the TDS is visible for violent [greater than the enhanced Fujita scale (EF)-3] tornadoes, but recently the signature has been observed by KOUN on 9 May 2007 in a tornado that received an EF-1 rating. The TDS is observed in at least six storms from the dataset (8 May 2003, 9–10 May 2003, 29–30 May 2004, 1 March 2007, 29 March 2007, and 9 May 2007), associated with tornadoes ranging in intensity from EF-1 to EF-4. The signatures were present for various durations while a tornado was on the ground, but each dissipated within 5–10 min after the tornado ended.

The polarimetric TDS provides additional utility when the tornado is not observable visually. If a tornado is completely wrapped in rain or occurs at night, storm spotters on the ground may not be able to confirm the presence of a tornado. These situations are especially dangerous because there may not be reports to verify the location or track of a tornado. If debris is lofted, though, the consequent TDS is a clear confirmation of such a tornado. In the rain-wrapped case, it is possible that raindrops may mix with the tornadic debris. If this happens, the Z_{DR} may be increased by the presence of liquid drops, resulting in a lack of a clearly defined TDS in Z_{DR}. However, the presence of any nonmeteorological scatterers, such as debris in a mixture with hydrometeors, will cause a considerable decrease in ρ_{HV}. Accordingly, one should be cautious about overemphasizing Z_{DR} in polarimetric tornado detection (e.g., Bluestein et al. 2007) in the presence of raindrops. In agreement with Ryzhkov et al. (2005a), ρ_{HV} is found to be the most powerful polarimetric variable for tornado detection.

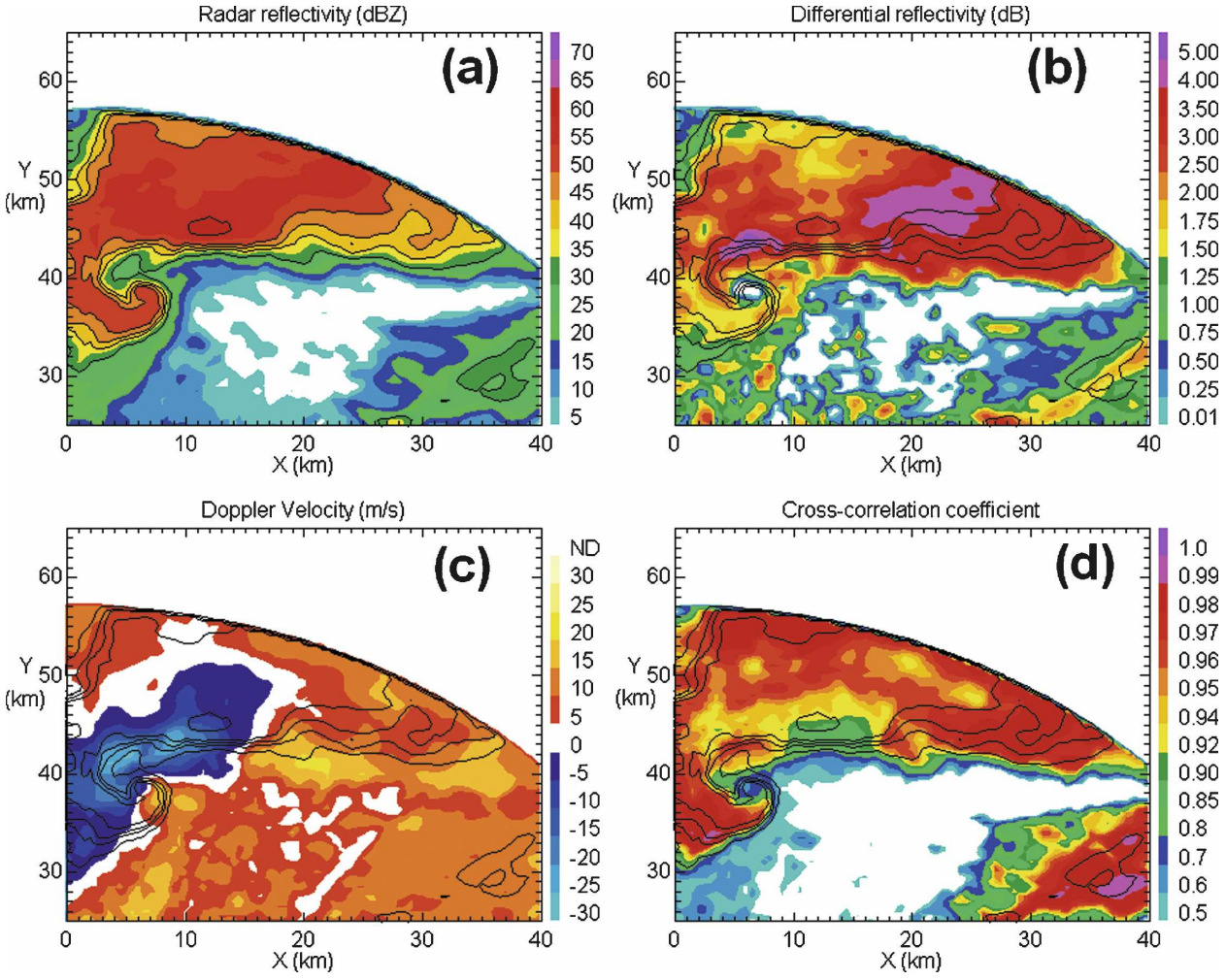

FIG. 2. Polarimetric radar variables at 0346 UTC 10 May 2003, shown on a 0.50-km CAPPI: (a) reflectivity factor (Z_{HH}; dBZ), (b) differential reflectivity (Z_{DR}; dB), (c) base Doppler velocity v_r (m s^{-1}), and (d) cross-correlation coefficient (ρ_{HV}). A TDS is seen at the tip of the hook echo, located at about $x = 6$ km, $y = 38$ km. Contours of Z_{HH} (dBZ; 30, 40, 45, 50, and 60) are overlaid on each of the panels to provide reference. These will be the contours for the rest of the figures unless otherwise noted.

b. Hail signature in the forward-flank downdraft

Hail is ubiquitous in supercell thunderstorms. Previous studies have shown that supercell updrafts are conducive to large hail production because growth to large sizes requires prolonged residence time in the moisture-rich updraft (Miller et al. 1988). Dry hailstones are well known to have polarimetric characteristics distinct from raindrops. Raindrops are modeled as oblate spheroids and are well oriented, and the oblateness of the raindrops increases with diameter (Pruppacher and Pitter 1971). Thus, in rain, high Z_{HH} is associated with high Z_{DR}. Hail smaller than about 1.5–2.0 cm that becomes wet tends to acquire either a water shell or torus of water (Rasmussen et al. 1984; Rasmussen and Heymsfield 1987), which stabilizes its orientation, changes its aspect ratio, and increases its refractive index. Therefore, small, wet hailstones are sensed as giant raindrops, characterized by very high Z_{DR}. In contrast, large hailstones tend to be drier; even in wet growth regimes they acquire a substantially thinner water coating, usually less than about 0.5 mm. Therefore, large hailstones tend to tumble (Lesins and List 1986), resulting in a rather chaotic orientation. Hence, the intrinsic Z_{DR} of large hail is close to 0.

The observed Z_{DR} depends on the relative contribution from raindrops, smaller wet hailstones, and larger hail to the scatterers in the resolution volume. At S band, a drop in Z_{DR} and an increase in Z_{HH} associated with an overwhelming contribution of large hailstones are routinely observed in the middle of hail shafts. The area of low Z_{DR} is typically surrounded by very high values of Z_{DR} associated with smaller wet hail and big raindrops originating from melting hailstones (e.g.,

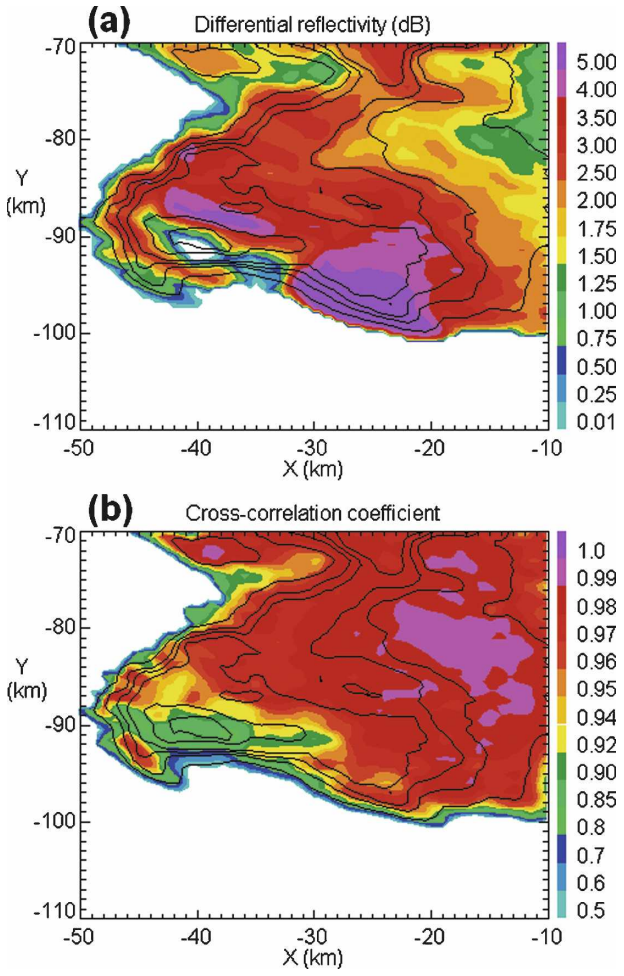

FIG. 3. Polarimetric signature of hail reaching the ground as shown in this 0.0° PPI at 2355 UTC 19 May 2003. The hail signature is centered at $x = -40$ km, $y = -92$ km. Polarimetric radar variables shown are (a) Z_{DR} and (b) ρ_{HV}. Contours of Z_{HH} are overlaid, as in Fig. 2.

Smyth and Illingworth 1998). Thus, high Z_{HH} and low Z_{DR} at the lowest tilt are good indicators (at S band) of hail reaching the ground. In the case of extremely large, irregularly shaped hailstones or rain mixed with hail, ρ_{HV} can also be substantially reduced (Balakrishnan and Zrnić 1990). Important differences exist in the hail signature at C band, which will be discussed in section 4. In the remainder of this subsection, only the hail signature at S band is considered.

The most common location for this signature is just downstream of the mesocyclone (low-level Z_{HH} hook) in the FFD, as shown schematically in Fig. 1. In an example of an observed hail signature from a 19 May 2003 nontornadic supercell (Fig. 3), the hail core is clearly evident, located just north of the hook echo or Z_{HH} appendage on the southwest portion of the storm. Research storm intercept teams from the Joint Polarization Experiment (JPOLE; Ryzhkov et al. 2005b) provided ground truth for this case. For a recent review and more examples of polarimetric hail detection and verification, see Heinselman and Ryzhkov (2006).

Each of the S-band cases was analyzed to investigate the frequency of occurrence of the hail signature. Van Den Broeke et al. (2008) report qualitatively that hail shafts as inferred from high Z_{HH} and low Z_{DR} are present most often at times leading up to tornadogenesis in the few cases they investigated. It is clear from the present analysis that the relationship between the hail signature appearance and tornado presence is weak and highly dependent on the individual storm characteristics, which can differ substantially in different climate regions; for example, Oklahoma (Great Plains) supercells produce very large hail more often than Alabama (Gulf Coast) storms (Doswell et al. 2005). In two of the tornadic supercells (10 November 2004 and 29 March 2007), the hail signature was absent throughout the entire storms' lifetime. This does not mean that hail was absent from these storms; in fact, small hail was reported on the ground and other polarimetric measurements, such as decreased ρ_{HV}, indicate mixed-phase hydrometeors, presumably rain mixed with hail or melting hail.

In the more typical warm season tornadic supercells (8 May 2003, 9–10 May 2003, and 29–30 May 2004), roughly 62% of the volume scans during which a tornado was on the ground exhibited a hail signature. Throughout the lifetime of the tornadic supercells, the hail signature was present in slightly more than half (52%) of the volume scans. A similar proportion of volume scans when no tornado was present also display the signature. Thus, our dataset provides evidence that the hail signature is present only slightly more frequently during tornadoes compared to the times before and after tornadoes. In the vast majority of the tornadic supercell cases, if the signature was present (absent) in the time leading up to tornadogenesis, it generally remained present (absent) after the tornado touched down.

In nontornadic supercells, the hail signature is present in just under 85% of the volume scans throughout the mature lifetime (defined as when the storm attains a quasi-steady state with a persistent midlevel mesocyclone) of the storms. This difference between tornadic and nontornadic supercells is probably quite difficult to assess operationally, because it is a retrospective result. Nonetheless, the data exhibit a strong indication that nontornadic supercell thunderstorms are characterized by persistent hail signatures, whereas hail signatures are more intermittent in tornadic supercells. Trapp (1999) found that low-level mesocyclones

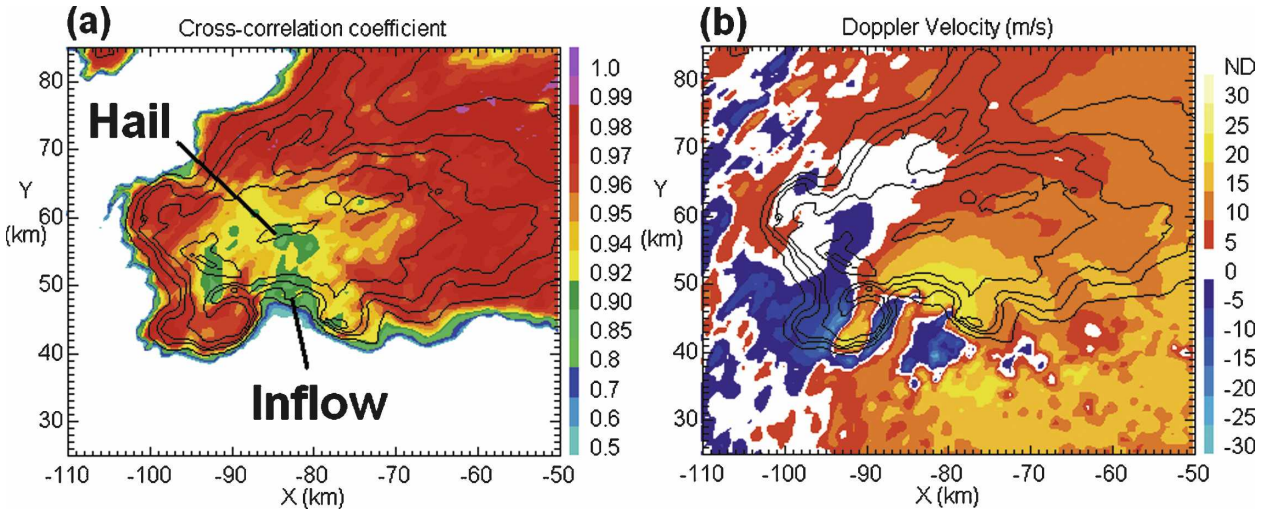

FIG. 4. PPI at 0.43° for 0023 UTC 30 May 2004, showing (a) the reduced ρ_{HV} as a result of light debris being ingested into the storm and hail at low levels and (b) the strong inflow evident in v_r. Contours of Z_{HH} are overlaid.

in tornadic supercells are characterized by smaller-core radii and greater vertical vorticity than mesocyclones in nontornadic supercells. The induced downward-directed perturbation pressure gradient force would then be stronger in tornadic supercells, weakening the updraft in tornadic supercells more than in nontornadic supercells. The weakening and occlusion of the main updraft into the divided mesocyclone phase has been considered a predecessor of tornadogenesis (e.g., Brandes 1978; Lemon and Doswell 1979; Houze 1993; Adlerman et al. 1999) and would not be as conducive to the production of large hail. Thus, we speculate that tornadic supercell updrafts are weakened to the extent that large hail production is inefficient more frequently than updrafts in nontornadic supercells. More detailed multi-Doppler analyses and numerical modeling must be done, however, to make any conclusive statements. A few of the nontornadic supercells were observed at large distances from the radar, so it is possible that the radar was sampling the storm at higher elevations where hail may not have melted fully. However, larger hail with large terminal velocities most likely will not melt appreciably before reaching the ground. We acknowledge this limitation of the data from these storms.

c. *Low-level inflow and updraft signatures*

Near-surface inflow into supercells can be intense (occasionally exceeding 25 m s^{-1}). Because of these strong winds, insects and/or other light debris, including grass, leaves, or dust, can be ingested into the storm updraft. This debris is characterized by irregular shapes and random orientation, which contribute to the drop in ρ_{HV}. The low-level inflow region along the FFD and reflectivity hook may then have a mixture of precipitation particles and nonmeteorological scatterers, subsequently reducing the ρ_{HV}. During the 30 May 2004 tornadic supercell, television news cameras captured video of light debris from a recently plowed field being ingested into the storm (T. J. Schuur 2006, personal communication). Both the inflow and hail signatures are present in ρ_{HV} (Fig. 4a), and strong inflow is evident in v_r (Fig. 4b). This signature is widespread and values of ρ_{HV} are usually above 0.7–0.8, as compared with a TDS (which typically has values of ρ_{HV} below 0.8), and thus should not be confused with the very localized and prominent TDS at the tip of the hook echo.

The ingestion of light debris into the main updraft is inferred by decreased ρ_{HV} aloft, collocated with the updraft. The decreased ρ_{HV} aloft can also be due to a lack of hydrometeors, which results in a low signal-to-noise ratio (<5 dB; Ryzhkov et al. 2005a), or to tumbling hailstones within or near the updraft core. Thus, in the absence of a clearly defined bounded weak-echo region (BWER), the area of decreased ρ_{HV} caused by any of these reasons may be used as a proxy for the updraft location. Additionally, Ryzhkov et al. (2005a) speculate that the lower value of ρ_{HV} may be an indirect measure of updraft strength.[1] An analysis of the cases in our dataset shows that both tornadic and nontornadic storms with particularly intense updrafts as deduced from extremely high echo tops and BWERs (e.g., 29–30 May 2004 and 10–11 April 2007) have sig-

[1] To confirm the updraft location and quantify its strength, dual-Doppler analyses and vertical velocity retrievals (which are beyond the scope of this paper) are necessary.

nificant ρ_{HV} depressions collocated with the BWERs and extend above the level at which the BWER fills in. The magnitude of ρ_{HV} in these "holes" is measured as low as 0.80–0.85. Even in less vertically extensive storms (e.g., 8 May 2003, 10 May 2003, 26 May 2004, and 10 November 2004), ρ_{HV} within the updraft occasionally drops to between 0.85 and 0.90 at times during the storm evolution.

d. Z_{DR} arc signature

Perhaps the most striking low-level feature in the right-moving supercells considered herein is the Z_{DR} arc signature, which occurs on the right (usually the southern) edge of the FFD, as shown in Fig. 1. Examples from several supercells in Oklahoma are shown in Fig. 5. The signature is shallow, generally less than 1–2 km in depth, and is not collocated with the Z_{HH} maximum. Instead, it is usually found along the maximum gradient of Z_{HH}. The Z_{DR} values in excess of 4–5 dB are not uncommon at S band and may be even higher at C band, for reasons explained in section 4. Antenna beam pattern mismatching has been ruled out because the signature is not observed along any other gradient in Z_{HH}. Instead, such high Z_{DR} values are associated with very large, oblate raindrops and a relative lack of smaller drops. To produce such a modified drop size distribution (DSD), size sorting of the raindrops must occur. The size-sorting mechanism in this case is the vertical increase in speed and veering of the storm-relative winds that occurs in right-moving supercell environments (Kumjian and Ryzhkov 2007), within which smaller raindrops that fall with smaller terminal velocities are advected farther from their source region than larger raindrops that fall faster. The different drop trajectories produced by the low-level wind shear result in a region of large drops on the southern edge of the FFD. Near the main updraft, vertical velocities may also contribute to the size sorting of drops.

One may attribute the origin of large drops in convective storms to the melting of hail or graupel. However, even though this may explain the origin of the drops, it does not fully explain why the signature is observed only on the southern edge of the FFD. Size sorting caused by veering wind profiles with height can explain the appearance and location of this signature for any DSD, given it is not monodispersed. It is important to point out that the Z_{DR} arc has been observed at S and C bands, and in different climate regions, including Oklahoma (all supercell cases in this dataset), Canada (19 August 2005), and the maritime environment of southern Alabama (15 November 2006 and 1 March 2007). The Z_{DR} arc has also been apparent in data from supercell case studies in Germany (Höller et al. 1994) and recently in Finland (Outinen and Teittinen 2007). Additionally, the signature has appeared in different seasons ranging from early March through November. The fact that the signature is present in varying locations and seasons strongly suggests that the size-sorting mechanism is intrinsic to supercell thunderstorms.

Kumjian and Ryzhkov (2007) show through a simple numerical model that the strength of the Z_{DR} arc signature (i.e., the degree of size sorting) is positively related to low-level storm-relative environmental helicity (SREH; see Davies-Jones et al. 1990),

$$\text{SREH} = \int_0^{z'} (\mathbf{v}_H - \mathbf{c}) \cdot \boldsymbol{\nabla} \times \mathbf{v}_H \, dz, \qquad (1)$$

where $\mathbf{v}_H$ is the horizontal velocity vector, $\mathbf{c}$ is the storm motion vector, and z' is an altitude that dictates the depth of the atmosphere over which the integration takes place. Typically, z' is taken to be about 3 km, representing the storm-inflow depth (Davies-Jones et al. 1990; Droegemeier et al. 1993; Markowski et al. 1998). SREH is a measure of the streamwise component of environmental vorticity. In order for thunderstorms to acquire midlevel rotation, the vorticity usually has a significant streamwise component (Davies-Jones 1984).

Typically, ordinary nonsevere convective storms do not display such a signature, though they may display a locally enhanced Z_{DR} region associated with an updraft. The updraft Z_{DR} enhancement is associated with a column (section 2e), whereas the Z_{DR} arc is a very shallow, elongated signature along the peak reflectivity gradient on the edge of the FFD. Thus, it should be easy to distinguish between these two polarimetric features. If a nonsupercell thunderstorm exhibits a Z_{DR} arc, it may indicate that the storm is experiencing enhanced SREH, which could lead to the ingestion of an increased component of streamwise vorticity. An example case of a tornadic nonsupercellular Oklahoma storm in which a Z_{DR} arc signature was observed preceding the development of a tornado is discussed in section 3.

e. Z_{DR} columns

The prominence of Z_{DR} columns associated with thunderstorm updrafts has caused these polarimetric features to be among the first reported in the literature (e.g., Caylor and Illingworth 1987; Conway and Zrnić 1993; Brandes et al. 1995). Columns in supercells are relatively narrow (4–8 km wide) and typically extend several kilometers above the environmental freezing level and are indicative of a positive temperature perturbation associated with the updraft. The high values

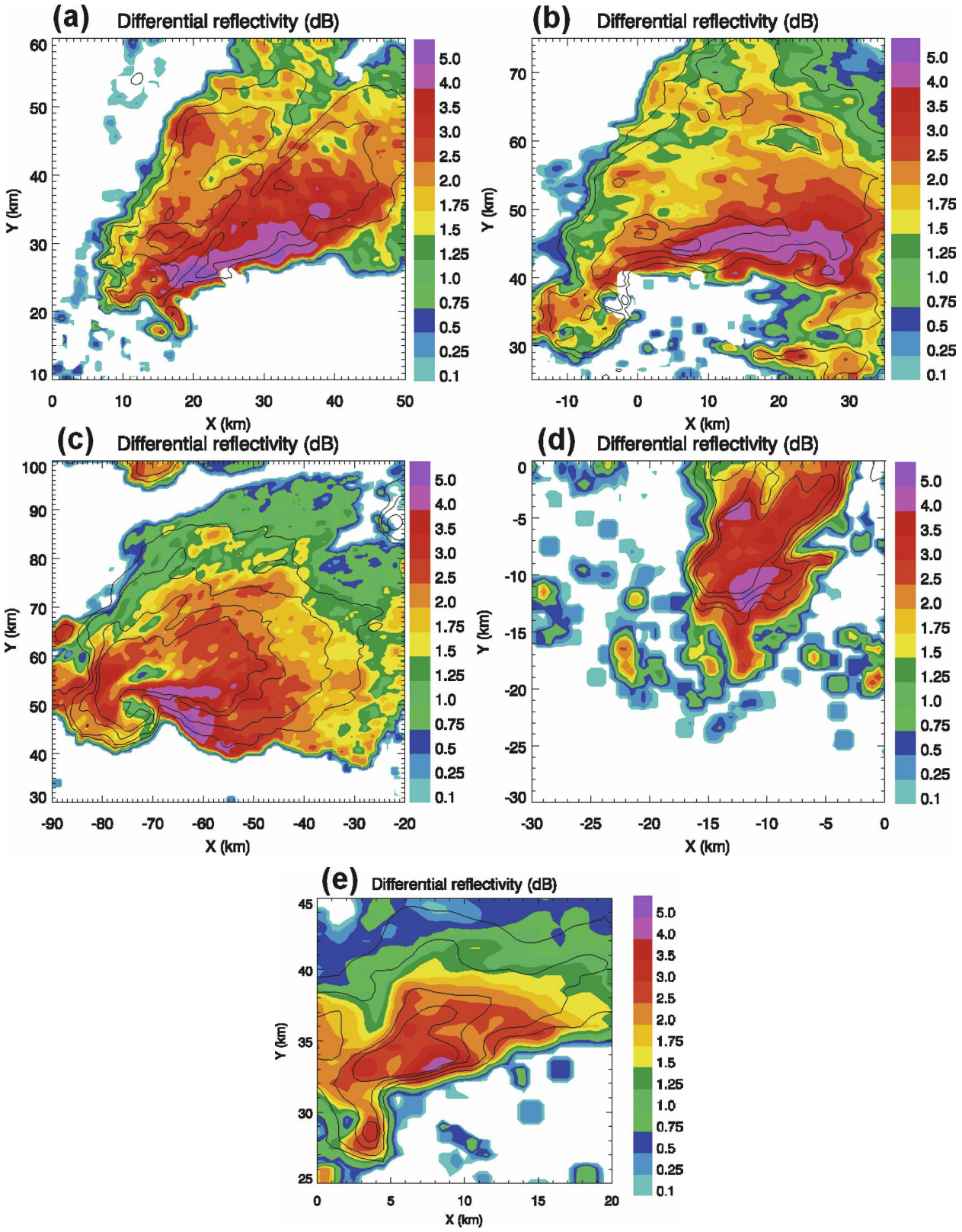

FIG. 5. Low-level PPI scans showing the Z_{DR} arc signature, located along the southern or inflow edge of the FFD, at (a) 2234 UTC 8 May 2003, taken at 1.5°; (b) 0333 UTC 10 May 2003, taken at 0.5°; (c) 0044 UTC 30 May 2004, taken at 0.5°; (d) 2354 UTC 10 Apr 2005, taken at 1.5°; and (e) 2228 UTC 10 Nov 2004, taken at 1.5°. Contours of Z_{HH} are overlaid.

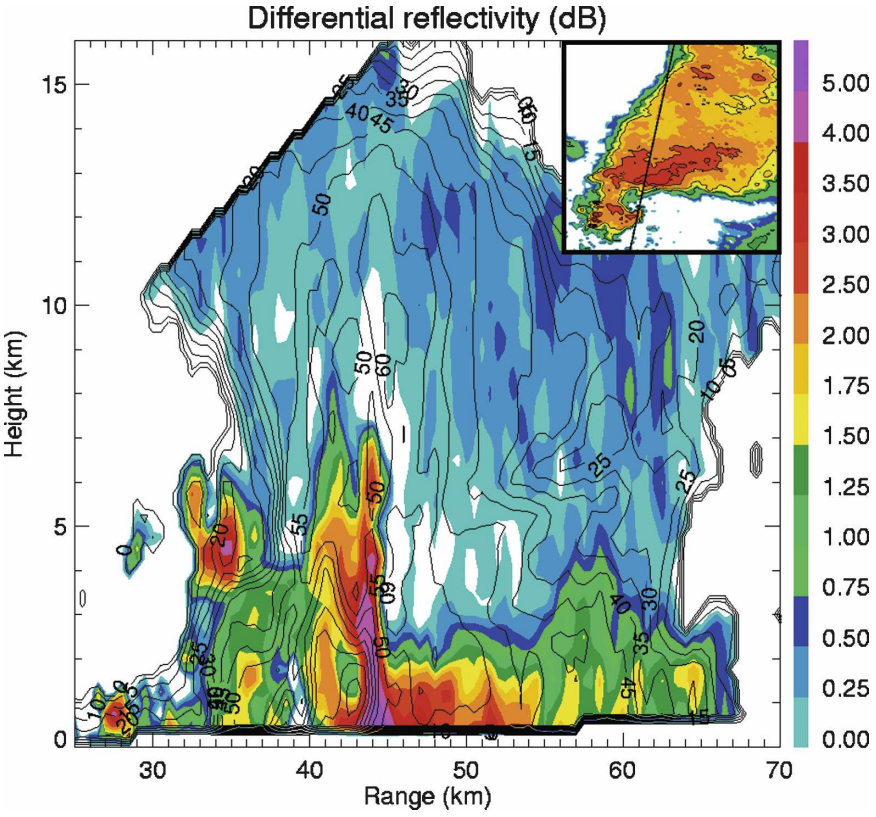

FIG. 6. A prominent Z_{DR} column is displayed at a range of about 44 km in this vertical cross section through the supercell at 0346 UTC 10 May 2003 through the 10° azimuth. A region of high positive values of Z_{DR} (>2 dB) extends up to about 7 km. The column can be seen clearly on the fringe of the BWER, which marks the updraft. Also, note the tornado debris signature at a range of 39.5 km. Contours of Z_{HH} are overlaid and annotated. The inset shows where the cross section is taken relative to the lowest-level PPI scan of Z_{HH}. Note the scales for range and height: the cross section is vertically stretched to emphasize the vertical extent of the column.

of Z_{DR} (>3 dB) indicate the presence of large, oblate hydrometeors, presumably either large raindrops or water-coated hailstones. Aircraft penetrations used in Brandes et al. (1995) and Loney et al. (2002) confirm that the Z_{DR} columns are made of a small number of large (>2 mm) raindrops and a few water-coated hailstones with a relative lack of smaller (<2 mm) drops. The origin of these drops has been explained through warm-rain collision and coalescence processes (e.g., Caylor and Illingworth 1987; Illingworth et al. 1987; Tuttle et al. 1989; Meischner et al. 1991) or from melting ice particles from the upwind Z_{HH} overhang or back-sheared anvil that are caught in low-level inflow and ingested back into the updraft (e.g., Conway and Zrnić 1993; Hubbert et al. 1998; Loney et al. 2002). In all of the previous studies and the storms analyzed for this paper, the Z_{DR} column is consistently found on the inflow side of the storm within or on the fringe of the updraft, as inferred from the BWER or inflow notch.

An example of a Z_{DR} column in the 10 May 2003 tornadic supercell is shown in a vertical cross section (Fig. 6). Regions of large positive values (>2 dB) extend to about 7 km, which is well above the environmental freezing level. Note that the Z_{DR} column is located on the periphery of the BWER, which marks the main updraft. The supercell updraft is so intense that nearly all hydrometeors are lofted and unable to fall. At the periphery of the main updraft where the magnitude of the vertical velocity is diminished the largest raindrops and coated hailstones begin to fall, enhancing the Z_{DR}. This is consistent with Conway and Zrnić (1993) and Loney et al. (2002), who found the maximum values of Z_{DR} to be coincident with weaker vertical velocities in the updraft. Kennedy et al. (2001) also found the Z_{DR} column to be within and immediately downstream of the center of the updraft in an intense convective hailstorm. In weaker updrafts or less-sheared environments one would expect the centers of

the updraft and Z_{DR} column to be more aligned as less horizontal (downstream) advection takes place. Thus, in general, the Z_{DR} column can be considered a proxy for the updraft.

A few studies (e.g., Hubbert et al. 1998) have noted a temporal evolution of the Z_{DR} column; specifically, the Z_{DR} values in the column were enhanced when the updraft was intensifying. Strengthening Z_{DR} columns in developing convective cells may indicate strengthening updrafts and could be considered a diagnosis of storm intensification. Additionally, the strength or prominence of Z_{DR} columns in multicellular convection may allow forecasters to distinguish between the decaying cells and those that are intensifying.

Because of the low vertical and temporal resolutions at high elevation angles in the scanning strategies used to collect data in this study, it is difficult to quantify small changes in the height of Z_{DR} columns. Although occasional sharp decreases or increases in height on the order of about 1 km between volume scans occurred, there is no obvious relationship between these changes and tornadogenesis.

f. K_{DP} columns

Similar to Z_{DR} columns, K_{DP} columns have been noted in the literature (e.g., Hubbert et al. 1998; Loney et al. 2002). These signatures are observed as columnar regions of enhanced positive K_{DP} in convective storms that frequently extend several kilometers above the freezing level. The K_{DP} column is generally found on the left flank of the updraft, spatially offset to the west or northwest of the Z_{DR} column. Despite the spatial offset of their centers, the K_{DP} and Z_{DR} columns can have a significant overlap (Fig. 1). Zrnić et al. (2001) present evidence that the Z_{DR} and K_{DP} columns in ordinary (nonsevere) convective storms are collocated; that is, there is no spatial offset. However, Schlatter (2003) describes a nonsupercellular convective storm that formed in a sheared environment north of a preexisting supercell that displayed the same spatial offset of the columns as the supercell storm to its south. This indicates that the offset is possibly related to the environmental shear or updraft strength. In a cursory analysis of ordinary convective thunderstorms in environments characterized by low shear, the centers of the K_{DP} and Z_{DR} columns were found to be collocated. High-resolution numerical modeling using explicit microphysics may help resolve this issue, which remains uncertain.

There are significant differences in the number and type of hydrometeors present in the K_{DP} and Z_{DR} columns in supercells. In contrast to Z_{DR} columns, in situ measurements presented in Loney et al. (2002) and Schlatter (2003) show that the K_{DP} column is associated with a high concentration of mixed-phase hydrometeors and is often collocated with high Z_{HH}. In general, K_{DP} columns are similar to columns of high Z_{HH}. The major difference is that Z_{HH} does not distinguish between liquid and frozen particles, whereas K_{DP} does. Other differences between the shapes of Z_{HH} and K_{DP} columns in rain or melting ice particles can be attributed to the following three reasons: K_{DP} is less weighted by large particles than Z_{HH}, K_{DP} is difficult to estimate in the presence of substantial backscatter differential phase δ, and K_{DP} estimates are prone to errors because of nonuniform beam filling, which can be significant in supercells. Because of the high concentration of smaller (1–2 mm) drops found in the K_{DP} column, Hubbert et al. (1998) take this signature to mark the presence of a region of drops shedding off hailstones. Because of the high liquid water content and positive temperature perturbation associated with the midlevel updraft, wet growth and subsequent shedding is likely in this part of the storm (Lesins and List 1986; Rasmussen and Heymsfield 1987). However, Loney et al. (2002) show that the enhancement of K_{DP} values in the column is dominated by contributions from larger (>2 mm) mixed-phase hydrometeors. Thus, K_{DP} columns as well as Z_{HH} columns are associated with a high concentration of raindrops and wet graupel or hail with a broad range of sizes, whereas the Z_{DR} columns mark regions with large raindrops and wet graupel or hail with a relative deficit of smaller hydrometeors.

A strong K_{DP} column is evident in a vertical cross section through the 10 May 2003 supercell (Fig. 7), centered on a range of 46 km. The region of large positive values ($>2^\circ$ km^{-1}) extends to a height of about 6.5 km. The column is clearly separated spatially from the BWER. One must take the difference in azimuth angle into consideration when comparing Figs. 6 and 7, so it is important to note that the K_{DP} column here is located to the north and west of the BWER and the Z_{DR} column. Like Z_{DR} columns, K_{DP} columns are persistent features throughout the mature lifetime of supercells. The region characterized by 1° km^{-1} values of K_{DP} generally extends at least as high as the 1-dB Z_{DR} column, in some cases extending 1–2 km higher. No clear relationship between fluctuations in vertical extent and strength and tornadogenesis were found in the dataset.

g. Midlevel Z_{DR} and ρ_{HV} rings

In both tornadic and nontornadic supercell thunderstorms a midlevel semicircular or circular ring of enhanced Z_{DR} and depressed ρ_{HV} is occasionally found above the environmental melting layer and most likely near the updraft-perturbed melting layer, which can be

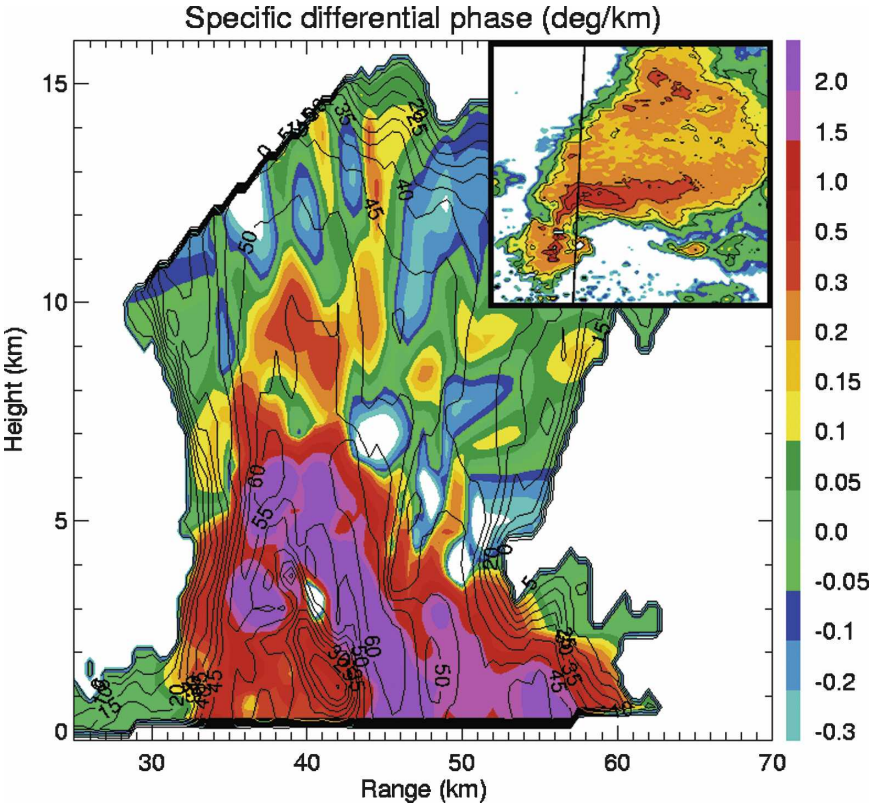

FIG. 7. A K_{DP} column is displayed at a range of about 46 km in this vertical cross section through the supercell at 0340 UTC 10 May 2003 along the 2° azimuth. Regions of high positive values of K_{DP} (>2° km^{-1}) extend up to about 6.5 km. Contours of Z_{HH} are overlaid and annotated. The inset shows where the cross section is taken relative to the lowest-level PPI scan of Z_{HH}. Note the scales for range and height: the cross section is vertically stretched to emphasize the vertical extent of the column.

crudely estimated using a sounding (for the spring cases, the perturbed melting layer is ~5 km above ground level). The signatures are not always present throughout the lifetime of the storm, but when they appear they can be striking (Figs. 8 and 9).

The fact that the rings are generally spatially offset from one another hints at an analog to the polarimetric melting layer signature, which has been documented in the literature (Ryzhkov and Zrnić 1998; Brandes and Ikeda 2004; Giangrande et al. 2005; Ikeda et al. 2005). The midlevel (4–6 km) updraft represents a positive temperature perturbation, whereas outside of the updraft at this level the polarimetric variables clearly indicate subfreezing temperatures and ice phase particles, such as graupel. Hydrometeors falling along the periphery of the updraft would then melt partially or completely, causing a distinct polarimetric signature. Mixed-phase and resonance-sized hydrometeors in this region would cause a decrease in ρ_{HV}, and the resulting water-coated ice particles would become increasingly oblate and have a higher dielectric constant as the fractional water volume increases, the effects of which would be to enhance Z_{DR} in the warmer air. Note that in some cases the enhanced Z_{DR} and depressed ρ_{HV} are only half-rings (e.g., Figs. 8d and 9a). When only half of a ring is evident, it has thus far always been observed on the right flank of the updraft. This region is typically associated with midlevel inflow, as evident by the inflow notch (weak-echo region) sometimes present in Z_{HH} (Figs. 1, 8, and 9). Ice hydrometeors falling from upper levels of the storm could also be entrained or "recycled" (Conway and Zrnić 1993) by the midlevel inflow preferentially on the right flank of the updraft. Generally, Z_{HH} is high around the updraft (surrounding the BWER), which is also a characteristic "bright-band" signature caused by melting hydrometeors. Figure 10 depicts the polarimetric variables through such a ring from the 10 May 2003 supercell. It is clear that the maximum in Z_{DR} is offset from the minimum in ρ_{HV}, which lends credence to the melting signature hypothesis.

The circular or semicircular appearance of the Z_{DR}

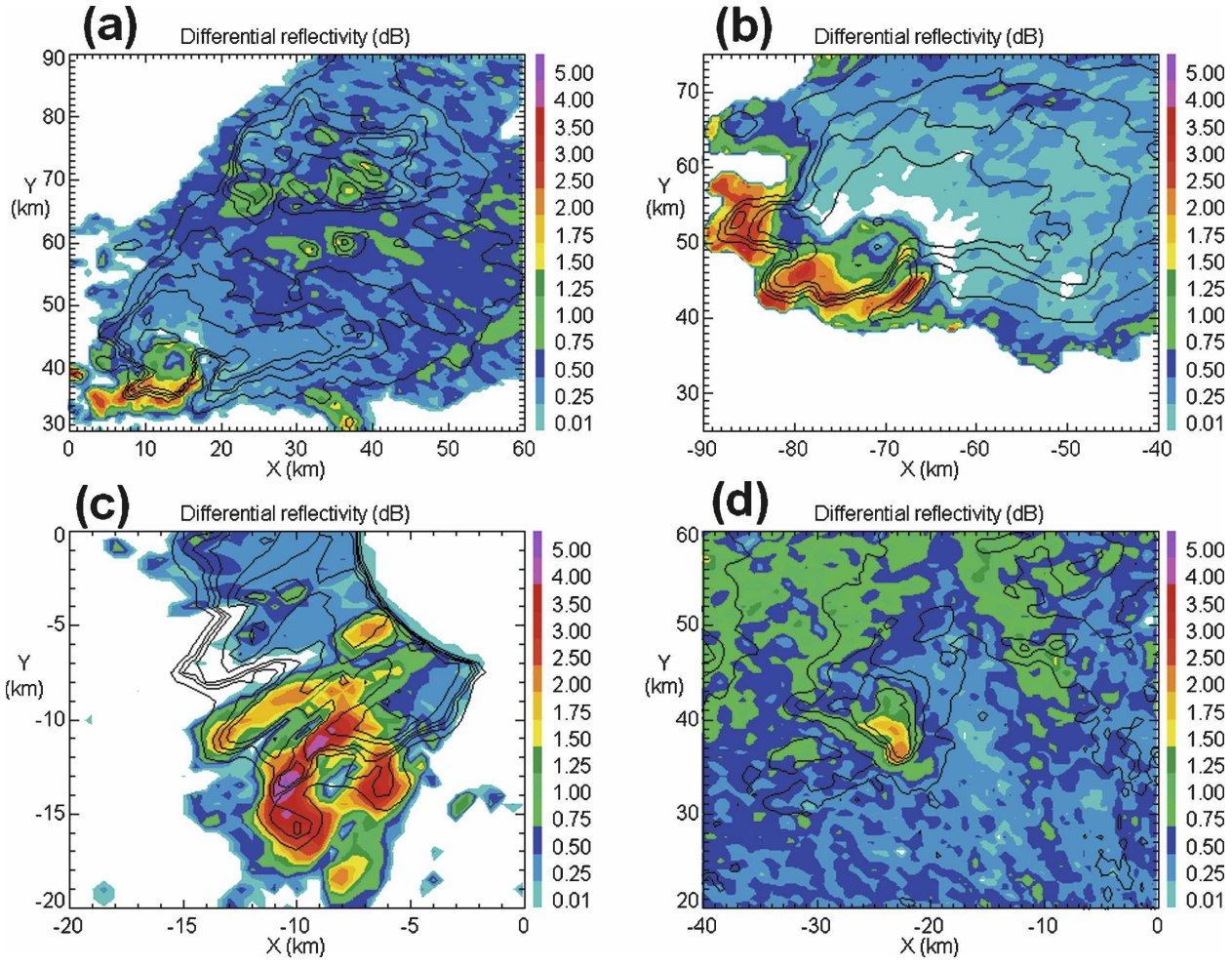

FIG. 8. Four examples of Z_{DR} rings at midlevels of the storms, plotted in CAPPIs at (a) 0351 UTC 10 May 2003, taken at 5.0 km; (b) 0044 UTC 30 May 2004, taken at 4.0 km; (c) 2354 UTC 10 Apr 2005, taken at 2.5 km; and (d) 2106 UTC 29 Mar 2007, taken at 4.0 km. Contours of Z_{HH} are overlaid.

and ρ_{HV} rings and their relative location to the updraft and mesocyclone suggest that they are associated with cyclonic vorticity. The cyclonic curvature could be explained by melting ice particles or large drops entrained from the FFD or from the Z_{DR} column being wrapped around by the mesocyclone. This would result in a cyclonically curved enhancement of Z_{DR} and a decrease in ρ_{HV}. Though centrifuging raindrops out of tornadoes can cause ringlike structures in radar variables (Dowell et al. 2005), the length and velocity scales of mesocyclones result in the rather weak centrifuging of raindrops. Only when rotation is strong (such as on the scale of a tornado) will the centrifuging of raindrops have an observable effect on polarimetric variables.

In addition to melting, midlevel entrainment of dry air would evaporate smaller precipitation particles on the periphery of the updraft, enhancing Z_{DR}. The mixing of environmental air near the updraft must be confined to a narrow ring as observed in the polarimetric variables. This description is similar to the "deep convergence zone" ("DCZ"), a narrow region of strong shear and turbulent mixing reported in some studies (e.g., Lemon and Parker 1996; Bluestein and Gaddy 2001), but the ring signature tends to be confined to a much smaller depth than the DCZs in the literature. Trajectory analyses and the modeling of explicit microphysics could provide more conclusive evidence and should be completed to determine if any of these hypotheses are true. No obvious relationship between these midlevel rings and tornadogenesis was found in our dataset.

3. Example application at S band: 9 May 2007

In this section we will highlight the applicability of the supercell polarimetric signatures to a nonsupercel-

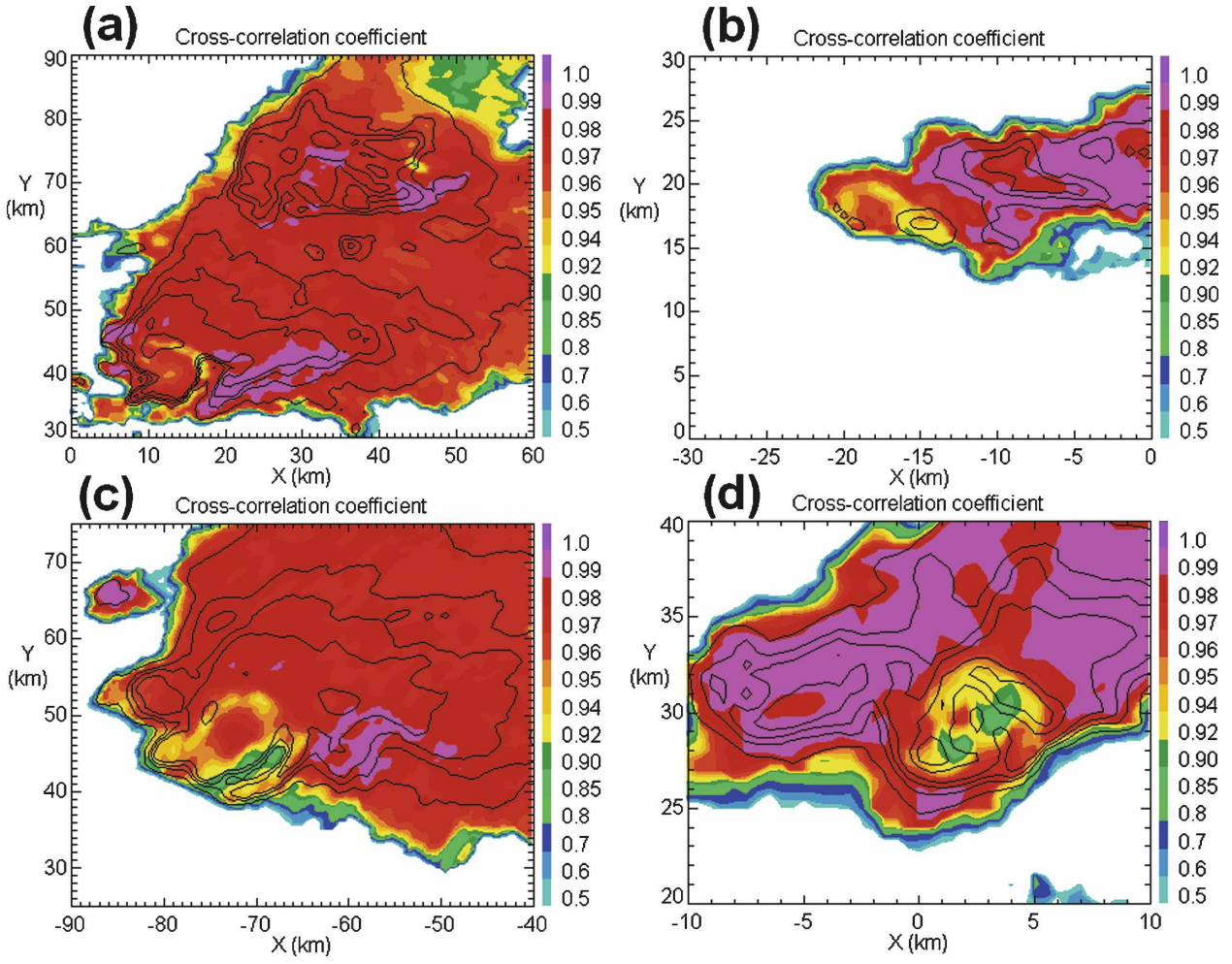

FIG. 9. Four examples of ρ_{HV} rings at midlevels of the storms, plotted in CAPPIs at (a) 0351 UTC 10 May 2003, taken at 5.0 km; (b) 0025 UTC 27 May 2004, taken at 4.75 km; (c) 0044 UTC 30 May 2004, taken at 5.5 km; and (d) 2221 UTC 10 Nov 2004, taken at 2.5 km. Contours of Z_{HH} are overlaid, as in previous figures.

lular storm that became tornadic. On 9 May 2007, a mesoscale convective vortex (MCV) evolved from earlier multicellular convection over western Oklahoma. At 0422 UTC, a weak Z_{DR} arc was evident along the southern edge of a cell embedded in the convective system (Fig. 11). The appearance of the Z_{DR} arc demonstrates that this particular storm cell could be experiencing enhanced SREH and thus should be closely monitored for signs of rotation. At 0436 UTC, a midlevel Z_{DR} half-ring appeared (Fig. 12a), indicating that there may be midlevel cyclonic vorticity present with the cell. The Doppler velocity field in Fig. 12b indicates a slight enhancement in the broad-scale rotation associated with the MCV; however, the broad cyclonic rotation associated with the MCV (inferred from Doppler velocity measurements) obscured the smaller-scale mesocyclone signature. Throughout the analyzed time, Z_{DR} and K_{DP} columns were present in the stronger cells, with their centers misaligned as described above. Seven minutes later (at 0443 UTC) the cell produced a tornado that caused high-end EF-1 damage in El Reno, Oklahoma. According to the official National Weather Service damage survey, the tornado was on the ground for approximately 7 min. The KOUN low-level scan during which the tornado was on the ground began at 0447 UTC, at which time a TDS is clearly evident in anomalously low values of ρ_{HV} (<0.80) and a Doppler vortex signature in v_r, located at approximately $x = -45$ km and $y = 31$ km in Fig. 13. The TDS does not show up in Z_{DR}, most likely because the tornado was embedded in rain. Further aloft, a Z_{DR} ring and a weak ρ_{HV} ring are present.

In a case like 9 May 2007, operational meteorologists would benefit from the use of polarimetric data. De-

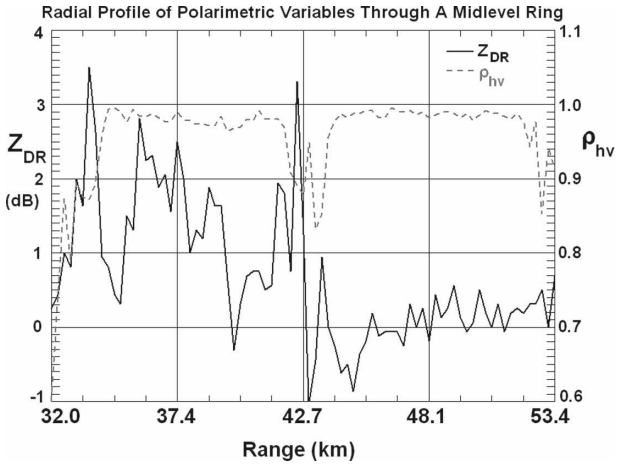

FIG. 10. Radial trace of Z_{DR} and ρ_{HV} through midlevel rings in the supercell at 0351 UTC 10 May 2003. The trace is at the 20° azimuth, at an elevation of 6.5°. The scale for Z_{DR} (solid black line; dB) is plotted on the left vertical axis, and the scale for ρ_{HV} (dashed gray line) is plotted on the right vertical axis. The edge of the storm is at a range of 32 km, corresponding to the beginning of the plot.

spite somewhat ambiguous signatures in v_r and Z_{HH} prior to tornadogenesis, the polarimetric signatures are quite similar to those observed in supercells. These similarities indicate that certain microphysical and kinematic mechanisms intrinsic to supercells, such as size sorting resulting from veering wind shear and the development of updraft rotation, may be happening in this nonsupercell storm. Forecasters could use such evidence to complement the Doppler velocity data in order to provide earlier and more confident warnings of storm severity and potential for tornado development. Once a tornado does form, the TDS provides unambiguous evidence that a damaging tornado is on the ground. Such a signature is particularly helpful in this case because the tornado was embedded in rain and occurred at night.

4. Measurements at C band

Interpretation of C-band polarimetric radar measurements requires special considerations resulting from more intense attenuation and pronounced effects of resonance scattering at shorter radar wavelengths. Resonance effects cause large raindrops (exceeding 4.5–5 mm) and hailstones to behave as Mie scatterers. Thus, if such large hydrometeors exist in the radar resolution volume, Z_{HH} and Z_{DR} can be significantly different from those observed at S band. Additionally, ρ_{HV} in pure rain (which usually exceeds 0.98 at S band) can drop as low as 0.93 at C band (Ryzhkov and Zrnić 2005).

These differences between observations at different wavelengths become important when interpreting the supercell thunderstorm polarimetric signatures presented in this study, especially the low-level hail signature at C band. Even with significant concentrations of large, dry hail (which is common in supercells), large raindrops and melting hailstones may cause the resulting Z_{DR} to remain high. In fact, Ryzhkov et al. (2007a) showed that in 11 storms from Canada and Alabama, there were no cases of a noticeable drop in Z_{DR} accompanied with high Z_{HH} where hail, some of it as large as baseballs, was reported on the ground. Despite the intrinsic near-zero Z_{DR} of large, tumbling hailstones

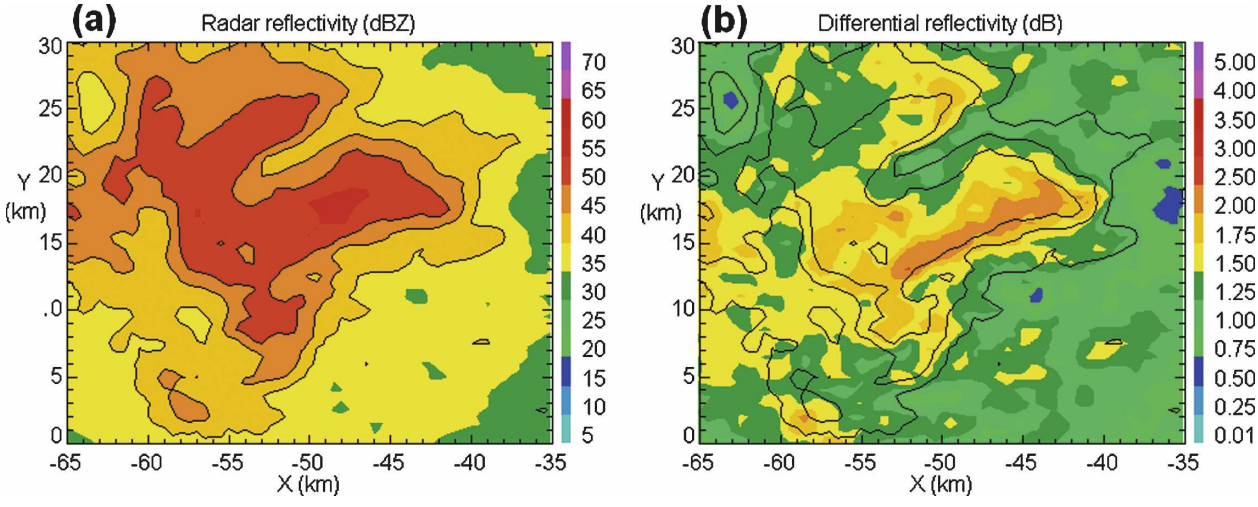

FIG. 11. The 0422 UTC 9 May 2007 0.75-km CAPPI, showing a weak Z_{DR} arc, evident along the gradient in Z_{HH} as a narrow region with $Z_{DR} > 2$ dB. Variables shown are (a) Z_{HH} and (b) Z_{DR}. The 40-, 45-, and 50-dBZ contours of Z_{HH} are overlaid on each panel.

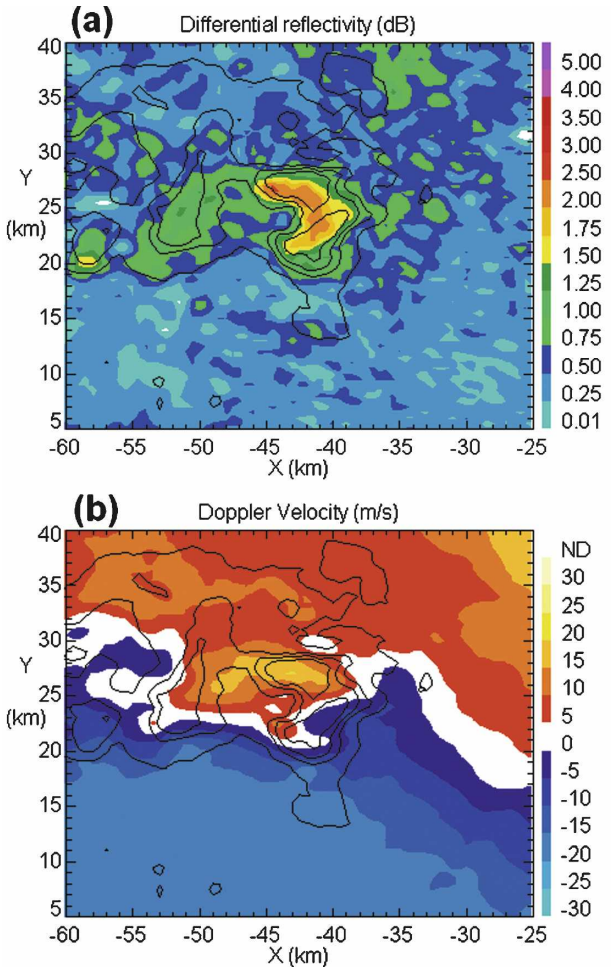

FIG. 12. The 0436 UTC 9 May 2007 4.5-km CAPPI of a midlevel Z_{DR} half-ring: (a) Z_{DR} and (b) base Doppler velocity, v_r. The 40-, 45-, and 50-dBZ contours of Z_{HH} are overlaid on each panel.

present in most supercells, the resulting Z_{DR} is generally dominated by the contributions from smaller melting hail and large raindrops, both of which produce anomalously high Z_{DR} at C band.

Additionally, hail cores in severe storms may produce very strong differential attenuation at C band, resulting in a tremendous drop of Z_{DR} on the rear side of the storm. However, if differential attenuation is correctly accounted for, the unbiased Z_{DR} remains high everywhere in the core. Significant decreases of Z_{DR} in hail cores at C band reported in some previous studies (e.g., Meischner et al. 1991; Höller et al. 1994) might be primarily attributed to differential attenuation. The attenuation correction algorithm suggested and validated by Ryzhkov et al. (2006, 2007b) accounts for regions in storms such as hail cores where anomalously high differential attenuation occurs. These regions can be small in spatial extent but can be responsible for a significant proportion of the differential attenuation.

The C-band measurements of ρ_{HV} suffer from stronger impacts of nonuniform beam filling (NBF). If the gradient of total differential phase Φ_{DP} becomes too large, NBF will manifest itself in a precipitous drop in ρ_{HV}. The effects of NBF are more prominent at shorter wavelengths because Φ_{DP} and its gradients are inversely proportional to wavelength, and the ρ_{HV} bias is inversely proportional to the square of the wavelength (Ryzhkov 2007). As the magnitude of ρ_{HV} decreases, the statistical errors and noisiness of the other polarimetric variables increase, degrading the quality of polarimetric data (Bringi and Chandrasekar 2001). Ryzhkov (2007) provides an example of NBF at S band as the radar beam is propagating down the length of a squall line, which is an infrequent situation, but one in which there is tremendous attenuation. In more common configurations the effects of the shorter wavelength are apparent in strong ρ_{HV} bias caused by NBF as well as significant differential attenuation.

The characteristic ρ_{HV} is low in rain at C band and is more negatively biased by NBF. Thus, it is sometimes difficult to use ρ_{HV} to distinguish between rain, hail, and nonmeteorological scatterers. The anomalously high Z_{DR} at C band resulting from the effects of resonance scattering will cause other differences in the supercell polarimetric signatures described above. Signatures in Z_{DR}, such as the low-level arc, columns, and midlevel rings, may become more prominent. Compared to S band, the observed values of Z_{DR} in supercell signatures at C band are higher (>6 dB in some cases).

1 March 2007—Enterprise, Alabama, tornado

In this section, data from the 1 March 2007 tornadic supercell in Enterprise will be presented. The EF-4 tornado caused horrific destruction and loss of life in the city, killing nine people and injuring dozens more. Damage estimates place the total cost between $200 and $300 million. The tornado came within 5 km of the Sidpol C-band polarimetric radar in Enterprise, passing just to its west and north. The extremely close range and high-resolution polarimetric measurements (125-m radial resolution) combine to form a unique dataset.

Several of the polarimetric signatures presented in this paper are readily apparent in the data. However, because of the close range of the storm, the middle and upper levels of the storm were not adequately sampled throughout the period of observations, even by the highest tilt (19.5°). Nevertheless, the low-level signatures are quite striking.

At the beginning of the analysis (1824 UTC), a prominent Z_{DR} arc is evident at low levels (not shown),

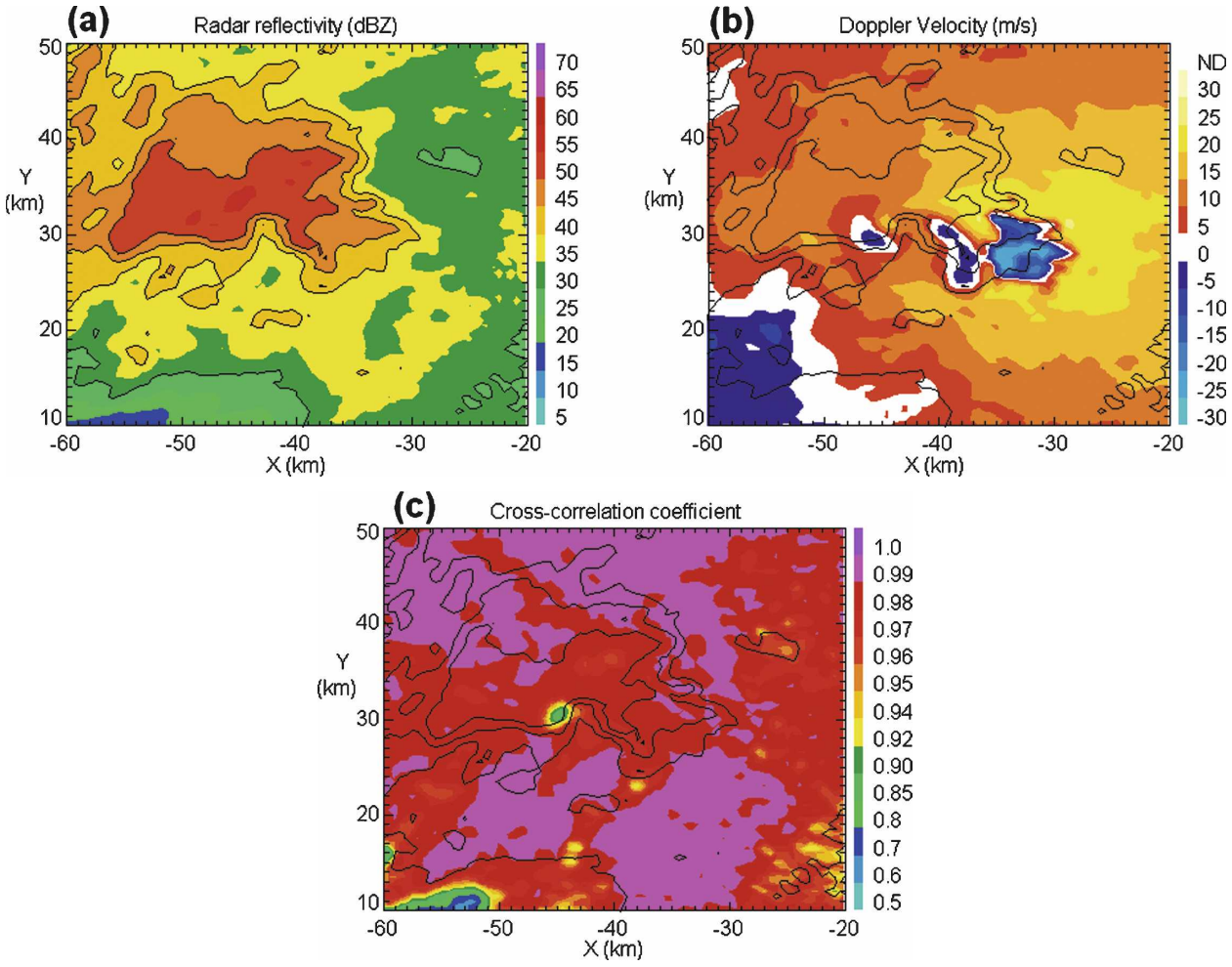

FIG. 13. The 0447 UTC 9 May 2007 0.75-km CAPPI, showing a TDS in the following variables: (a) Z_{HH}, (b) v_r, and (c) ρ_{HV}. There is no indication of a tornado in (a), but a Doppler vortex signature is present in (b) at about $x = -45$ km, $y = 31$ km, which is collocated with anomalously low values of ρ_{HV} (TDS) in (c). The 40-, 45-, and 50-dBZ contours of Z_{HH} are overlaid on each panel.

and this signature remained present throughout the lifetime of the storm. At midlevels, a BWER in Z_{HH}, a Z_{DR} ring, and a ρ_{HV} half-ring are present after proper attenuation correction is applied (Fig. 14). All of these are consistent with the supercellular nature of the storm and are analogous to the signatures presented in section 2 from S-band observations. Over the next several volume scans, the storm became better organized as it approached Enterprise. The first tornado developed around 1908 UTC, after which it intensified and hit Enterprise High School at about 1912 UTC. The data from this time show a clear TDS at the tip of the hook echo in Fig. 15. Despite the high (5.5°) elevation angle, the radar is still sampling the storm at low altitudes (<1 km) because of its close proximity. Also apparent in Fig. 15 is the strong Z_{DR} arc signature in the FFD, with values in excess of 6 dB; a narrow region of values in excess of 3 dB is clearly seen wrapping around the inside of the hook echo.

5. Discussion and summary

In most existing storm-scale numerical models, size sorting and explicit microphysics are not fully accounted for with the use of bulk microphysics schemes. Instead, computed quantities like liquid water mixing ratio along with assumed raindrop and hailstone size distributions are used to calculate radar variables. The assimilation of dual-polarization data into storm-scale models will benefit forecasts if the model is able to reproduce the observed polarimetric signatures. Unfortunately, this is rather difficult for bulk microphysics parameterization schemes. If the models cannot reproduce the polarimetric signatures described here, then

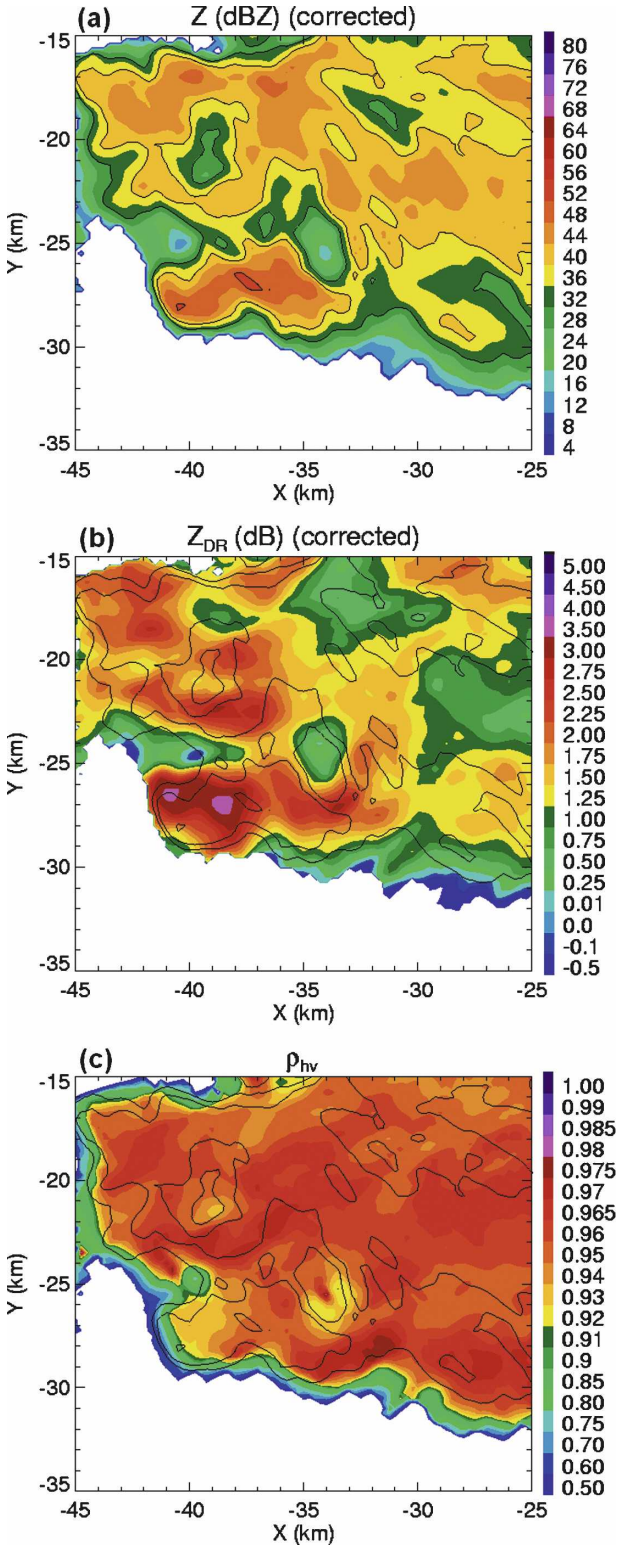

FIG. 14. The 1827 UTC 1 Mar 2007 5.5° PPI in Enterprise. Corrected fields of (a) Z_{HH}, (b) Z_{DR}, and (c) ρ_{HV} are shown. Contours of Z_{HH} (32, 40, and 52 dBZ) are overlaid. The rings are centered at about $x = -34$ km, $y = -25$ km.

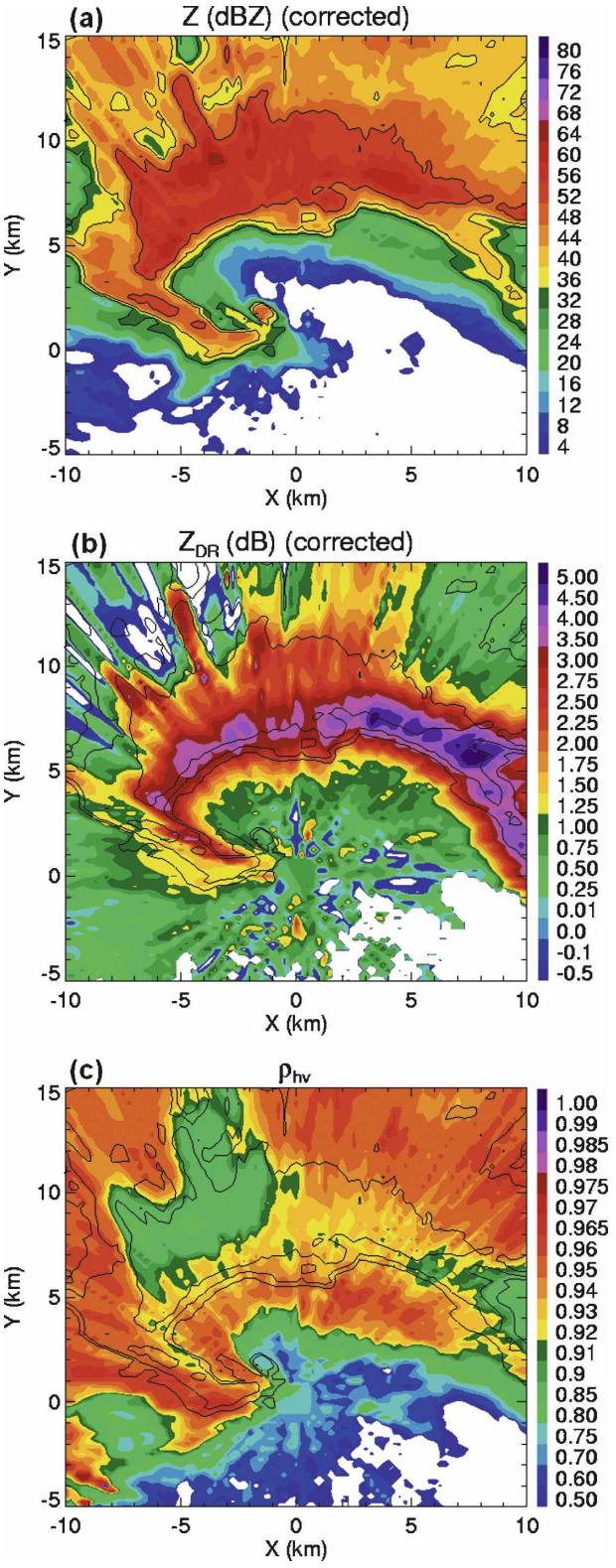

FIG. 15. As in Fig. 14, except for 5.5° PPI from 1912 UTC, while the tornado is on the ground causing EF-4 damage. The TDS is evident at the tip of the hook echo (approximately $x = -1$ km, $y = 2$ km) and the low-level Z_{DR} arc is quite prominent, with Z_{DR} values as high as 4 dB wrapping around the inside of the hook echo.

they do not fully capture the intrinsic microphysics of supercell storms.

The signatures presented herein may provide operational meteorologists with an additional nowcasting tool. The low-level features can aid forecasters with more precise warning locations and verifications (i.e., pinpoint tornado and hail warnings), as well as reveal information about storm behavior and evolution. Perhaps the most promising signature presented is the Z_{DR} arc. The Z_{DR} arc is indicative of a kinematic property of supercell storms, so it is unique in that it can be seen through polarimetric observations of the microphysical process of size sorting in the storm. We should emphasize that this is not just an azimuthal shear signature like a Doppler velocity couplet or tornado vortex signature (TVS); instead, the arc signature indicates a *vertical* shear. In an operational setting it is very difficult to view this type of veering from Doppler velocities, and it is fundamentally impossible to assess vertical shear profiles from the Doppler velocities of one elevation scan. To assess the vertical profile of winds in the storm, one must either compare different tilts simultaneously (which is time consuming in an operational setting) or make use of velocity azimuth displays (VADs), which can be inaccurate in inhomogeneous environments with isolated convective storms.

Strong veering of the storm-relative wind (large values of SREH) is usually associated with severe weather. Many studies (e.g., Fawbush and Miller 1954; Maddox 1976; Darkow and McCann 1977; Davies-Jones 1984) have established the relationship between storm intensity and speed and directional shear of the storm-relative winds. Thus, the Z_{DR} arc signature could be an indication of enhanced SREH, and more importantly an indicator of storm severity. A Z_{DR} arc appearing in a nonsupercellular convective storm may indicate the potential onset of updraft rotation (a mesocyclone). Once midlevel vorticity is produced, other polarimetric signatures described in this paper, such as the midlevel Z_{DR} ring, may possibly be used in conjunction with Doppler velocity data to confirm the onset of storm-scale rotation. The persistence of the hail signature at low levels could provide insight on the tornado potential of the supercell in some cases. Middle- and upper-level features indicative of updraft strength (Z_{DR} and K_{DP} columns, ρ_{HV} hole, etc.) can alert forecasters to storm intensity.

The fact that these features are present in supercells in different climate regions provides evidence that they are manifestations of intrinsic microphysical and kinematic processes in all supercell thunderstorms. The capability of polarimetric radar to observe these processes offers clues about storm behavior, undoubtedly a useful complement to conventional single-polarization Doppler radar data. Quantitative analysis of the signatures presented here through trajectory analyses, DSD retrievals, and explicit microphysical modeling must be done to fully understand the processes inferred from polarimetric radar observations.

Most of the obvious and prominent polarimetric signatures (except the TDS) do not provide a clear distinction between tornadic and nontornadic supercells. The challenge is to find polarimetric precursors of tornadogenesis, which will require more comprehensive quantitative analysis of the growing dataset. The qualitative nature of this study precludes any definitive answers to the problem of tornadogenesis. At this time, the dynamics of supercell tornadogenesis and tornadogenesis failure are still unknown. If microphysics plays a role, polarimetric radar measurements may aid in elucidating the enigmatic processes associated with tornadogenesis.

Acknowledgments. This work evolved from part of an M.S. thesis at the University of Oklahoma and is supported under the NSF Grant ATM-0532107. Additional funding was provided by NOAA/Office of Oceanic and Atmospheric Research under NOAA/University of Oklahoma Cooperative Agreement NA17RJ1227, U.S. Department of Commerce. The authors thank the NSSL/CIMMS employees who maintain and operate the KOUN polarimetric radar for research-grade applications. We are also grateful for the polarimetric data from Environment Canada, Weather Decision Technologies, Inc., and Enterprise Electronics Corporation. Alan Shapiro and Kevin Scharfenberg reviewed the manuscript and helped to clarify several aspects of our analysis. Additionally, useful discussions with Dusan Zrnić, Terry Schuur, Tian Yu, Gabriel Garfield, Scott Giangrande, Alex Schenkman, and Matthew Van Den Broeke aided the completion of this study. Comments from three anonymous reviewers aided in improving this work.

REFERENCES

Adlerman, E. J., K. K. Droegemeier, and R. Davies-Jones, 1999: A numerical simulation of cyclic mesocyclogenesis. *J. Atmos. Sci.,* **56,** 2045–2069.

Balakrishnan, N., and D. S. Zrnić, 1990: Use of polarization to characterize precipitation and discriminate large hail. *J. Atmos. Sci.,* **47,** 1525–1540.

Biggerstaff, M. I., and Coauthors, 2005: The Shared Mobile Atmospheric Research and Teaching Radar: A collaboration to enhance research and teaching. *Bull. Amer. Meteor. Soc.,* **86,** 1263–1274.

Bluestein, H. B., and S. G. Gaddy, 2001: Airborne pseudo-dual-

Doppler analysis of a rear-inflow jet and deep convergence zone within a supercell. *Mon. Wea. Rev.,* **129,** 2270–2289.

——, A. L. Pazmany, J. C. Galloway, and R. E. Mcintosh, 1995: Studies of the substructure of severe convective storms using a mobile 3-mm-wavelength Doppler radar. *Bull. Amer. Meteor. Soc.,* **76,** 2155–2169.

——, M. M. French, R. L. Tanamachi, S. Frasier, K. Hardwick, F. Junyent, and A. Pazmany, 2007: Close-range observations of tornadoes in supercells made with a dual-polarization, X-band, mobile Doppler radar. *Mon. Wea. Rev.,* **135,** 1522–1543.

Brandes, E. A., 1977: Flow in a severe thunderstorm observed by dual-Doppler radar. *Mon. Wea. Rev.,* **105,** 113–120.

——, 1978: Mesocyclone evolution and tornadogenesis: Some observations. *Mon. Wea. Rev.,* **106,** 995–1011.

——, 1981: Finestructure of the Del City–Edmond tornadic mesocirculation. *Mon. Wea. Rev.,* **109,** 635–647.

——, 1984a: Relationships between radar-derived thermodynamic variables and tornadogenesis. *Mon. Wea. Rev.,* **112,** 1033–1052.

——, 1984b: Vertical vorticity generation and mesocyclone sustenance in tornadic thunderstorms: The observational evidence. *Mon. Wea. Rev.,* **112,** 2253–2269.

——, and K. Ikeda, 2004: Freezing-level estimation with polarimetric radar. *J. Appl. Meteor.,* **43,** 1541–1553.

——, R. Davies-Jones, and B. C. Johnson, 1988: Streamwise vorticity effects on supercell morphology and persistence. *J. Atmos. Sci.,* **45,** 947–963.

——, J. Vivekanandan, J. D. Tuttle, and C. J. Kessinger, 1995: A study of thunderstorm microphysics with multiparameter radar and aircraft observations. *Mon. Wea. Rev.,* **123,** 3129–3143.

Bringi, V. N., and V. Chandrasekar, 2001: *Polarimetric Doppler Weather Radar: Principles and Applications*. Cambridge University Press, 636 pp.

——, T. A. Seliga, and W. A. Cooper, 1984: Analysis of aircraft hydrometeor spectra and differential reflectivity (Z_{DR}) radar measurements during the Cooperative Convective Precipitation Experiment. *Radio Sci.,* **19,** 157–167.

——, J. Vivekanandan, and J. D. Tuttle, 1986: Multiparameter radar measurements in Colorado convective storms. Part II: Hail detection studies. *J. Atmos. Sci.,* **43,** 2564–2577.

——, D. A. Burrows, and S. M. Menon, 1991: Multiparameter radar and aircraft study of raindrop spectral evolution in warm-based clouds. *J. Appl. Meteor.,* **30,** 853–880.

——, L. Liu, P. C. Kennedy, V. Chandrasekar, and S. A. Rutledge, 1996: Dual multiparameter radar observations of intense convective storms: The 24 June 1992 case study. *Meteor. Atmos. Phys.,* **59,** 3–31.

Browning, K. A., 1964: Airflow and precipitation trajectories within severe local storms which travel to the right of the winds. *J. Atmos. Sci.,* **21,** 634–639.

——, 1965: The evolution of tornadic storms. *J. Atmos. Sci.,* **22,** 664–668.

Cai, H., and R. M. Wakimoto, 2001: Retrieved pressure field and its influence on the propagation of a supercell thunderstorm. *Mon. Wea. Rev.,* **129,** 2695–2713.

Caylor, I. C., and A. J. Illingworth, 1987: Radar observations and modeling of warm rain initiation. *Quart. J. Roy. Meteor. Soc.,* **113,** 1171–1191.

Conway, J. W., and D. S. Zrnić, 1993: A study of production and hail growth using dual-Doppler and multiparameter radars. *Mon. Wea. Rev.,* **121,** 2511–2528.

Darkow, G. L., and D. W. McCann, 1977: Relative environmental winds for 121 tornado bearing storms. Preprints, *10th Conf. on Severe Local Storms,* Omaha, NE, Amer. Meteor. Soc., 413–417.

Davies-Jones, R., 1984: Streamwise vorticity: The origin of updraft rotation in supercell storms. *J. Atmos. Sci.,* **41,** 2991–3006.

——, D. W. Burgess, and M. Foster, 1990: Test of helicity as a forecast parameter. Preprints, *16th Conf. on Severe Local Storms,* Kananaskis Park, Alberta, Canada, Amer. Meteor. Soc., 588–592.

Doswell, C. A., 1994: Flash-flood-producing convective storms: Current understanding and research. *Proc. U.S.–Spain Workshop on Natural Hazards,* Barcelona, Spain, National Science Foundation, 97–107.

——, 2001: Severe convective storms—An overview. *Severe Convective Storms, Meteor. Mongr.,* No. 50, Amer. Meteor. Soc., 1–26.

——, H. E. Brooks, and M. P. Kay, 2005: Climatological estimates of daily local nontornadic severe thunderstorm probability for the United States. *Wea. Forecasting,* **20,** 577–595.

Doviak, R. J., and D. S. Zrnić, 1993: *Doppler Radar and Weather Observations*. Academic Press, 562 pp.

Dowell, D. C., C. R. Alexander, J. M. Wurman, and L. J. Wicker, 2005: Centrifuging of hydrometeors and debris in tornadoes: Radar-reflectivity patterns and wind-measurement errors. *Mon. Wea. Rev.,* **133,** 1501–1524.

Droegemeier, K. K., S. M. Lazarus, and R. P. Davies-Jones, 1993: The influence of helicity on numerically simulated convective storms. *Mon. Wea. Rev.,* **121,** 2005–2029.

Fawbush, E. J., and R. C. Miller, 1954: The types of airmasses in which North American tornadoes form. *Bull. Amer. Meteor. Soc.,* **35,** 154–165.

Gal-Chen, T., 1982: Errors in fixed and moving frame of references: Applications for conventional and Doppler radar analysis. *J. Atmos. Sci.,* **39,** 2279–2300.

Giangrande, S. E., A. V. Ryzhkov, and J. Krause, 2005: Automatic detection of the melting layer with a polarimetric prototype of the WSR-88D radar. Preprints, *32nd Int. Conf. on Radar Meteorology,* Albuquerque, NM, Amer. Meteor. Soc., 11R.2. [Available online at http://ams.confex.com/ams/pdfpapers/95894.pdf.]

Grzych, M. L., B. D. Lee, and C. A. Finley, 2007: Thermodynamic analysis of supercell rear-flank downdrafts from project ANSWERS. *Mon. Wea. Rev.,* **135,** 240–246.

Heinselman, P. L., and A. V. Ryzhkov, 2006: Validation of polarimetric hail detection. *Wea. Forecasting,* **21,** 839–850.

Herzegh, P. H., and A. R. Jameson, 1992: Observing precipitation through dual-polarization radar measurements. *Bull. Amer. Meteor. Soc.,* **73,** 1365–1374.

Höller, H., V. N. Bringi, J. Hubbert, M. Hagen, and P. F. Meischner, 1994: Life cycle and precipitation formation in a hybrid-type hailstorm revealed by polarimetric and Doppler radar measurements. *J. Atmos. Sci.,* **51,** 2500–2522.

Houze, R. A., 1993: *Cloud Dynamics*. Academic Press, 573 pp.

Hubbert, J., V. N. Bringi, L. D. Carey, and S. Bolen, 1998: CSU-CHILL polarimetric measurements from a severe hailstorm in eastern Colorado. *J. Appl. Meteor.,* **37,** 749–755.

Ikeda, K., E. A. Brandes, and R. M. Rasmussen, 2005: Polarimetric radar observations of multiple freezing levels. *J. Atmos. Sci.,* **62,** 3624–3636.

Illingworth, A. J., J. W. F. Goddard, and S. M. Cherry, 1987: Po-

larization radar studies of precipitation development in convective storms. *Quart. J. Roy. Meteor. Soc.,* **113,** 469–489.

Kennedy, P. C., and S. A. Rutledge, 1995: Dual-Doppler and multiparameter radar observations of a bow-echo hailstorm. *Mon. Wea. Rev.,* **123,** 921–943.

——, ——, W. A. Petersen, and V. N. Bringi, 2001: Polarimetric radar observations of hail formation. *J. Appl. Meteor.,* **40,** 1347–1366.

Klemp, J. B., and R. B. Wilhelmson, 1978: Simulations of right- and left-moving storms produced through storm splitting. *J. Atmos. Sci.,* **35,** 1097–1110.

Kumjian, M. R., and A. V. Ryzhkov, 2007: Polarimetric characteristics of tornadic and nontornadic supercell thunderstorms. Preprints, *33rd Conf. on Radar Meteorology,* Cairns, Queensland, Australia, Amer. Meteor. Soc., P10.1. [Available online at http://ams.confex.com/ams/pdfpapers/122882.pdf.]

Lemon, L. R., and C. A. Doswell, 1979: Severe thunderstorm evolution and mesocyclone structure as related to tornadogenesis. *Mon. Wea. Rev.,* **107,** 1184–1197.

——, and S. Parker, 1996: The Lahoma storm deep convergence zone: Its characteristics and role in storm dynamics and severity. Preprints, *26th Conf. on Radar Meteorology,* Norman, OK, Amer. Meteor. Soc., 206–208.

Lesins, G. B., and R. List, 1986: Sponginess and drop shedding of gyrating hailstones in a pressure-controlled icing wind tunnel. *J. Atmos. Sci.,* **43,** 2813–2825.

Loney, M. L., D. S. Zrnić, J. M. Straka, and A. V. Ryzhkov, 2002: Enhanced polarimetric radar signatures above the melting level in a supercell storm. *J. Appl. Meteor.,* **41,** 1179–1194.

Maddox, R. A., 1976: An evaluation of tornado proximity wind and stability data. *Mon. Wea. Rev.,* **104,** 133–142.

Markowski, P. M., 2002: Hook echoes and rear-flank downdrafts: A review. *Mon. Wea. Rev.,* **130,** 852–876.

——, J. M. Straka, E. N. Rasmussen, and D. O. Blanchard, 1998: Variability of storm-relative helicity during VORTEX. *Mon. Wea. Rev.,* **126,** 2959–2971.

——, ——, and ——, 2002: Direct surface thermodynamic observations within the rear-flank downdrafts of nontornadic and tornadic supercells. *Mon. Wea. Rev.,* **130,** 1692–1721.

Marwitz, J. D., 1972: The structure and motion of severe hailstorms. Part I: Supercell storms. *J. Appl. Meteor.,* **11,** 166–179.

Meischner, P. F., V. N. Bringi, D. Heimann, and H. Höller, 1991: A squall line in southern Germany: Kinematics and precipitation formation as deduced by advanced polarimetric and Doppler radar measurements. *Mon. Wea. Rev.,* **119,** 678–701.

Miller, L. J., J. D. Tuttle, and C. A. Knight, 1988: Airflow and hail growth in a severe northern High Plains supercell. *J. Atmos. Sci.,* **45,** 736–762.

Outinen, K., and J. Teittinen, 2007: Case study of a tornadic supercell in Finland 28 August, 2005. *Proc. Fourth European Conf. on Severe Storms,* Trieste, Italy, European Severe Storms Laboratory, 5.14. [Available online at http://essl.org/ECSS/2007/abs/05-Radars/1177940008.outinen-1-sec5.poster.pdf.]

Pruppacher, H. R., and R. L. Pitter, 1971: A semi-empirical determination of the shape of cloud and raindrops. *J. Atmos. Sci.,* **28,** 86–94.

Rasmussen, E. N., and A. J. Heymsfield, 1987: Melting and shedding of graupel and hail. Part I: Model physics. *J. Atmos. Sci.,* **44,** 2754–2763.

——, and J. M. Straka, 1998: Variations in supercell morphology. Part I: Observations of the role of upper-level storm-relative flow. *Mon. Wea. Rev.,* **126,** 2406–2421.

——, V. Levizzani, and H. R. Pruppacher, 1984: A wind tunnel and theoretical study on the melting behavior of atmospheric ice particles. III: Experiment and theory for spherical ice particles of radius >500 μm. *J. Atmos. Sci.,* **41,** 381–388.

Rotunno, R., and J. Klemp, 1982: The influence of the shear-induced pressure gradient on thunderstorm motion. *Mon. Wea. Rev.,* **110,** 136–151.

——, and ——, 1985: On the rotation and propagation of simulated supercell thunderstorms. *J. Atmos. Sci.,* **42,** 271–292.

Ryzhkov, A. V., 2007: The impact of beam broadening on the quality of radar polarimetric data. *J. Atmos. Oceanic Technol.,* **24,** 729–744.

——, and D. S. Zrnić, 1998: Discrimination between rain and snow with a polarimetric radar. *J. Appl. Meteor.,* **37,** 1228–1240.

——, and ——, 2005: Radar polarimetry at S, C, and X bands: Comparative analysis and operational implications. Preprints, *32nd Conf. on Radar Meteorology,* Albequerque, NM, Amer. Meteor. Soc., 9R.3. [Available online at http://ams.confex.com/ams/pdfpapers/95684.pdf.]

——, D. Burgess, D. Zrnić, T. Smith, and S. Giangrande, 2002: Polarimetric analysis of a 3 May 1999 tornado. Preprints, *22nd Conf. on Severe Local Storms,* Hyannis, MA, Amer. Meteor. Soc., 14.2. [Available online at http://ams.confex.com/ams/pdfpapers/47348.pdf.]

——, T. J. Schuur, D. W. Burgess, and D. S. Zrnić, 2005a: Polarimetric tornado detection. *J. Appl. Meteor.,* **44,** 557–570.

——, ——, ——, P. L. Heinselman, S. E. Giangrande, and D. S. Zrnić, 2005b: The Joint Polarization Experiment: Polarimetric rainfall measurements and hydrometeor classification. *Bull. Amer. Meteor. Soc.,* **86,** 809–824.

——, D. Hudak, and J. Scott, 2006: A new polarimetric scheme for attenuation correction at C band. *Proc. Fourth European Conf. on Radar in Meteorology and Hydrology,* Barcelona, Spain, Servei Meteorològic de Catalunya, 29–32.

——, and Coauthors, 2007a: Comparison of polarimetric algorithms for hydrometeor classification at S and C bands. Preprints, *33rd Conf. on Radar Meteorology,* Cairns, Queensland, Australia, Amer. Meteor. Soc., 10.3. [Available online at http://ams.confex.com/ams/pdfpapers/123109.pdf.]

——, P. Zhang, D. Hudak, J. L. Alford, M. Knight, and J. W. Conway, 2007b: Validation of polarimetric methods for attenuation correction at C band. Preprints, *33rd Conf. on Radar Meteorology,* Cairns, Queensland, Australia, Amer. Meteor. Soc., P11B.12. [Available online at http://ams.confex.com/ams/pdfpapers/123122.pdf.]

Schlatter, P. T., 2003: Polarimetric radar and in-situ measurements of a nontornadic supercell. M.S. thesis, School of Meteorology, University of Oklahoma, 97 pp.

Shabbott, C. J., and P. M. Markowski, 2006: Surface in situ observations within the outflow of forward-flank downdrafts of supercell thunderstorms. *Mon. Wea. Rev.,* **134,** 1422–1441.

Smith, J. A., M. L. Baeck, Y. Zhang, and C. A. Doswell III, 2001: Extreme rainfall and flooding from supercell thunderstorms. *J. Hydrometeor.,* **2,** 469–489.

Smyth, T. J., and A. J. Illingworth, 1998: Correction for attenuation of radar reflectivity using polarization data. *Quart. J. Roy. Meteor. Soc.,* **124,** 2393–2415.

Straka, J. M., E. N. Rasmussen, and S. E. Fredrickson, 1996: A mobile mesonet for finescale meteorological observations. *J. Atmos. Oceanic Technol.,* **13,** 921–936.

Thompson, R. L., R. Edwards, J. A. Hart, K. L. Elmore, and P. Markowski, 2003: Close proximity soundings within supercell

environments obtained from the Rapid Update Cycle. *Wea. Forecasting,* **18,** 1243–1261.

Trapp, R. J., 1999: Observations of nontornadic low-level mesocyclones and attendant tornadogenesis failure during VORTEX. *Mon. Wea. Rev.,* **127,** 1693–1705.

Tuttle, J. D., V. N. Bringi, H. D. Orville, and F. J. Kopp, 1989: Multiparameter radar study of a microburst: Comparison with model results. *J. Atmos. Sci.,* **46,** 601–620.

Van Den Broeke, M. S., J. M. Straka, and E. N. Rasmussen, 2008: Polarimetric radar observations at low levels during tornado life cycles in a small sample of classic southern plains supercells. *J. Appl. Meteor. Climatol.,* **47,** 1232–1247.

Wicker, L. J., and R. B. Wilhelmson, 1995: Simulation and analysis of tornado development and decay within a three-dimensional supercell thunderstorm. *J. Atmos. Sci.,* **52,** 2675–2703.

Wurman, J., J. M. Straka, E. N. Rasmussen, M. Randall, and A. Zahrai, 1997: Design and deployment of a portable, pencil-beam, pulsed, 3-cm Doppler radar. *J. Atmos. Oceanic Technol.,* **14,** 1502–1512.

Zrnić, D. S., and A. V. Ryzhkov, 1999: Polarimetry for weather surveillance radars. *Bull. Amer. Meteor. Soc.,* **80,** 389–406.

——, V. N. Bringi, N. Balakrishnan, K. Aydin, V. Chandrasekar, and J. Hubbert, 1993: Polarimetric measurements in a severe hailstorm. *Mon. Wea. Rev.,* **121,** 2223–2238.

——, A. V. Ryzhkov, J. Straka, Y. Liu, and J. Vivekanandan, 2001: Testing a procedure for automatic classification of hydrometeor types. *J. Atmos. Oceanic Technol.,* **18,** 892–913.